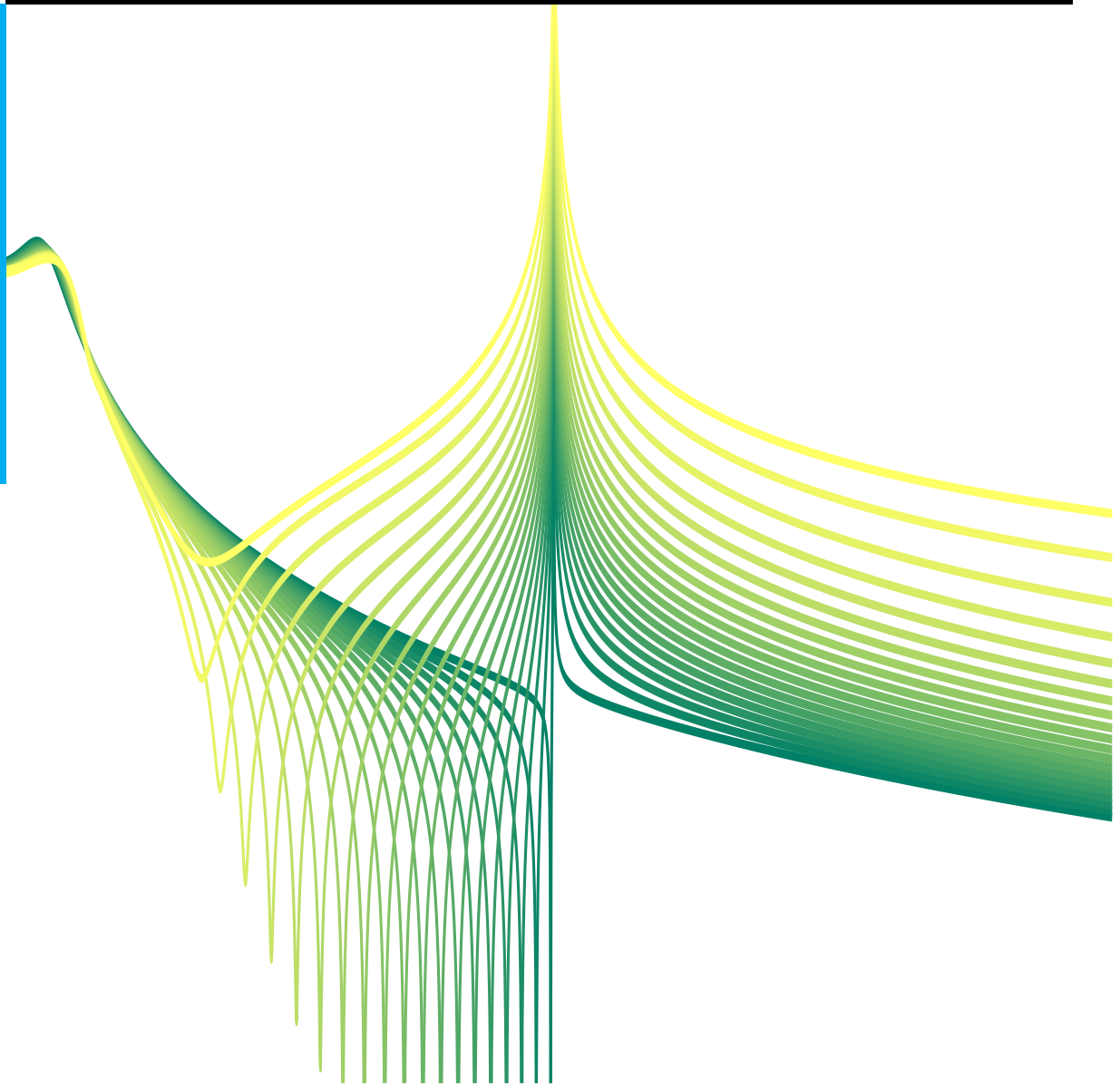


Skirt Decomposition Method for the Identification of Linear Time-Varying Human Joint Admittance

G. Cavallo

Master of Science Thesis



***Skirt Decomposition Method* for the Identification of Linear Time-Varying Human Joint Admittance**

by

Gaia Cavallo

For the double degree of Master of Science in Biomedical Engineering & Systems and
Control
at Delft University of Technology.

Student number: 4331591
Department : Biomedical Engineering
Systems & Control
Project duration: September 1, 2016 – July 7, 2017

Thesis committee:	Dr. Ir. A.C. Schouten	Chairman BME	BME, TU Delft
	Dr. Ir. J.W. van Wingerden	Chairman DCSC	DCSC, TU Delft
	Ir. M. van de Ruit,	Daily supervisor	BME, TU Delft
	Dr. Ing. R. Van de Plas	External Member	DCSC, TU Delft
	Dr. Ir. J. Lataire	External Member	Vrije Universiteit Brussel

An electronic version of this thesis is available at <http://repository.tudelft.nl/>.



Copyright © Biomedical Engineering & Systems and Control
All rights reserved.

Acknowledgements

Inevitably, I associate this Thesis with my experience in Delft. With this few words, I would like to express all my gratitude to everyone who took part in this adventure in The Netherlands. Getting to this point would not have been possible without the support of all the special people I met along the way.

Thanks to my supervisors, Alfred Schouten and Jan-Willem van Wingerden, for the guidance throughout the whole project. Your valuable advice and feedback were essential to carry on my Thesis and the lessons learned will prove of great help for my future career.

Thanks to my daily supervisor, Mark van de Ruit, for helping me patiently in every step of the project, providing me with technical and moral support. It was a pleasure working together.

Thanks to Eric Perreault, for welcoming me in your lab in Chicago. There I could experience in first person how an engineer can contribute to the quality of life of impaired patients. It provided important motivation for my work.

Thanks to the Professors who helped me from a distance. John Lataire, thank you for the fun, interesting conversations and for sharing your knowledge with me. Daniel Ludvig, thanks for supporting me and guiding me during my internship even though you were elsewhere.

Thanks to Martijn Vlaar, who supervised me on the literature study. Thanks for teaching me critical thinking.

Thanks to my family. You always motivated me to push my boundaries, to travel, to experience, and indirectly you are the main reason I am here today. Thanks to my mother, for the selfless affection and for being such a beautiful example of a woman, to my father, for teaching me to 'push the dot' always a bit further, to my sisters Flaminia and Livia, for coloring my life with a bit of foolishness.

Thanks to Marco, for fighting this together; we shared failures and achievements, and all of this wouldn't have been complete without you. You supported me every single day, and your trust in me gave me confidence and motivation to carry on.

Thanks to my housemates Sneha, Lily, and Lubo, because you had to witness all of the mood swings in the last period. The dinners together have been a fundamental element of my daily routine.

Thanks to my previous housemates, Jay and Quentino, which have become brothers to me. Thanks for all the amazing food, the conversations, the life lessons.

Thanks to Little Italy, which has been a small family in here. Thank you to Giorgio, Luca, Camilla, and Maria.

Thanks to my friends who came all the way here from Italy to celebrate together. Manu and Livietta for always being there, Barbara for being so capable of listening, Cati for your strength and comprehension, to me you are here as well today.

Thanks to the people who helped me in these last few days: Gurgio, for your delightful comments, Cheron, for always sharing a smile radiating energy, Frederik, for preventing me from falling down, Michiel, for sharing puns to keep me smile, Stijn, for the essentials coffee breaks, Alex, for making my text Canadian proof, and Pino, for the indirect help.

Thanks to all the people who passed by the Tower Power to have a day of study together. Your company made everything seem easier. Thanks to Sarvesh and Timo for being 'old' colleagues, good friends and a point of reference. Thanks to Sjors for the fun and kindness, thanks to Edo for being my study mate, thanks to Robin for bringing celebrations whenever you were around.

Thanks to my Ultimate team, for the all the time spent together in which I could switch off my mind for a bit.

Finally, to fulfill a promise I made a long time ago, thanks to Dario Farotto.

Preface

This thesis titled 'Skirt Decomposition Method for the Identification of Linear Time-Varying Human Joint Admittance' is submitted for the Double Degree of Master of Science at the Delft University of Technology, Netherlands. The research described herein was conducted under the supervision of Dr. Ir. A.C. Schouten, Dr. Ir. J.W. van Wingerden and Ir. M. van de Ruit in the Departments of Biomechanical Engineering and Systems and Control at the Faculty of Mechanical, Maritime and Materials Engineering. This work is to the best of my knowledge original, except where acknowledgments and references are made to previous work.

Gaia Cavallo
43331591
Delft University of Technology
7th July, 2017

GLOSSARY

BME	Biomedical Engineering
DCSC	Delft Center for Systems and Control
DOF	Degrees of Freedom
FRF	Frequency Response Function
IRF	Impulse Response Function
LPV	Linear Parameter-Varying
LTI	Linear Time-Invariant
LTV	Linear Time-Varying
MVC	Maximum Voluntary Contraction
MISO	Multiple-Input Single-Output
RMS	Root-Mean-Square
RMSE	Root-Mean-Square-Error
SI	System Identification
SNR	Signal-to-Noise ratio
VAF	Variance Accounted For

CONTENTS

I	Introduction	3
I-A	Identification of nonlinear joint admittance	3
I-B	Problem definition	4
I-C	Thesis objective	4
II	Skirt Decomposition Method	4
II-A	Modeling of LTV systems	4
II-B	Main identification steps	5
III	Simulation Study	6
III-A	Simulation method	6
III-A1	Simulink model	6
III-A2	Model and identification parameters	6
III-A3	Performance analysis	6
III-B	Simulation results	7
III-B1	Case studies 1,2,3	7
III-B2	Case study 4	7
III-C	Discussion on simulation study	7
III-C1	Effects of design parameters on simulation accuracy	7
III-D	Sub-conclusions on the simulation study	10
IV	Experimental Study	10
IV-A	Experimental method	10
IV-A1	Subjects	10
IV-A2	Setup	10
IV-A3	Task	10
IV-A4	Perturbation design	11
IV-A5	Pre-processing of the data	11
IV-A6	Data and performance analysis	12
IV-B	Experimental results	12
IV-B1	Input and output data	12
IV-B2	Estimation accuracy	13
IV-B3	Estimated signals	14
IV-C	Discussion on experimental study	15
IV-C1	Effects of design parameters on experimental accuracy	15
IV-C2	Model interpretation	16
IV-C3	Accuracy of the method	17
IV-D	Sub-conclusions on experimental study	17
V	Discussion	18
V-A	Time variation in the simulation and the experimental study	18
V-B	LTV identification of human joint admittance	18
V-C	<i>Skirt Decomposition</i> method on human joint admittance	18
VI	Conclusions	19
	References	19

Appendix A: Nonlinear Joint Admittance and Identification	23	
A-A	Physiology of joint admittance	23
A-A1	Intrinsic and reflexive properties	23
A-A2	Muscular contraction	24
A-B	Identification of joint admittance	24
A-B1	Experimental setup	24
A-B2	Challenges	25
Appendix B: LTV systems	26	
B-A	Definition	26
B-A1	Cause of the time variation	26
B-B	Response	27
B-B1	Impulse response function	27
B-B2	Sinusoidal response	27
B-B3	Response to a multisine signal	28
B-C	Nonparametric model	28
B-C1	LTV system function	28
B-C2	Polynomial decomposition	29
Appendix C: Skirt Decomposition Method	31	
C-A	Multisine Input signal	31
C-A1	Properties of the multisine	31
C-B	Rewriting the formula	31
C-C	Linear least-squares regression	33
C-D	Reconstruction of the LTV system function	33
C-E	Reconstruction of the output	33
C-F	Assumptions	34
Appendix D: Additional Figures and Tables	35	

Skirt Decomposition Method for the Identification of Linear Time-Varying Human Joint Admittance

Gaia Cavallo. Delft University of Technology, The Netherlands.

Abstract—Human joint admittance changes with numerous factors constituting the operational point. For large changes of the operational point, joint admittance can be identified using Linear Time-Varying methods on torque and angular position signals measured on human joints. Out of the available methods, the Skirt Decomposition method was selected due to its nonparametric structure and the limited number of *a priori* assumptions it makes. Its employment on the identification of human joint admittance was completely novel. The method was applied to a simulation model representing joint admittance and on experimental data measured from the wrist joint. In the experiment, the subjects were changing the applied torque to follow a desired trajectory, while the angle of the wrist was perturbed by the manipulator. With a properly designed multisine input, taking into consideration the speed and complexity of the time variation, a variance accounted for (VAF) close to 100 % was obtained in the simulation study on all the tested conditions. From the experiment, it was seen that the contribution of the time variation in the frequency domain was partially masked by the output noise. The noise level could be decreased by lowering the amplitude of the desired torque, and by removing the voluntary torque from the analyzed data. With a desired torque level ranging between 5% and 20%, and considering the bandwidth between 2 Hz and 20 Hz, the mean power of the output residuals in the frequency domain ranged between 16.2 and 27.1 for all the tested conditions. Furthermore, the time-varying dynamics retrieved from the system function showed a clear correlation with the desired torque trajectory.

I. INTRODUCTION

A. Identification of nonlinear joint admittance

In everyday tasks, the mechanical properties of the human body are in constant change to guarantee stability, optimality and effort minimization [42]. For instance, if a person hits an obstacle on the floor while walking, the person's reflexes will be activated to adjust the compliance of the lower limbs' joints and prevent falling [39]. The dynamic compliance of a joint is represented by joint admittance, a measure which explains how a joint reacts to external disturbances [12]. For different medical purposes it is useful to have a representation of joint admittance during motor activities. Knowing how joint admittance changes during functional tasks can be useful to design powered prosthetic joints that adjust their properties by mimicking the dynamic behavior of human joints [35]. The incorporation of artificial components with variable admittance would improve the mobility of prosthetic devices, rendering motor tasks more stable and more natural

for the users [10], [35]. Furthermore, the realization of a model of joint admittance could be used for the diagnosis of motor disorders. It is believed that impairments such as dystonia, tremors and bradykinesia [32], [34], [36], [39] are related to abnormal control of the reflexive component of joint admittance. The comparison of the behavior of impaired and unimpaired subjects could provide a tool to understand the pathophysiology of the disorders and to diagnose them analytically [31].

To build a model of joint admittance, System Identification (SI) methods can be used, starting from torque and position measurements obtained experimentally from human joints. Traditionally, a small amplitude input is applied around a fixed operational point, and joint admittance is identified using Linear Time-Invariant (LTI) methods [29], [34], [43]. The resulting model only provides a local approximation, since in reality joint admittance is nonlinear and varies with the operational point. There are in fact several physiological and mechanical factors that affect joint admittance nonlinearly [14], [15], [41]. Joint angle, activation level, and muscular fatigue are a few known examples:

- In a multibody system, a change in the joint angle can alter the inertia perceived at the joint, since a change of geometrical configuration affects the apparent mass [8].
- A change in the joint angle alters the level of stretch of the surrounding tissues, causing a nonlinear change of their viscous and elastic properties [47].
- A change in the activation level results in a different probability of cross-bridges (microscopic elements in a muscle that determine its level of contraction (Appendix A-B), resulting in altered viscous and elastic properties of the joint [39], [47].
- During prolonged muscular contractions fatigue occurs, which reduces the maximal force that can be produced by a muscle.

To obtain a representation of joint admittance during functional tasks, the dependence on the operational point should be considered. Nevertheless, it is not feasible to have a white box representation of joint admittance and to understand how it is affected by changes in the operational point. The neuromuscular system is highly nonlinear, and each component of the operational point interacts with the others in unpredictable ways. A SI strategy to tackle the modeling problem is to assume that the changes of joint admittance are caused by the passage of time, rather than by alterations of the operational point. Under this assumption, joint admittance can be linearized with respect to time, which is a readily available, known measurement, and joint admittance can be represented by a Linear Time-Varying

Alfred Schouten: Supervisor from the BME department of TU Delft;
 Jan-Willem van Wingerden: Supervisor from the DCSC of TU Delft;
 Mark van de Ruit- Daily Supervisor from the BME department of TU Delft.

(LTV) model.

B. Problem definition

In literature there exist multiple methods that can be applied to LTV models, and they can be broadly classified as *subspace*, [30], [44] *prediction error* [4] and *nonparametric* methods [20], [23], [25]. In the first group, the system is represented in state-space form, and the fundamental dynamics are retrieved starting from Henkel matrices containing the measured data. In the second group, a predetermined parametric model is fit to the system by means of minimization of a cost function. In the last, the measured signals are used to retrieve non-parametrically the LTV Frequency Response Function (FRF) or the Impulse Response Function (IRF) of a system. The LTV methods have been mostly applied to the identification of LTV physical systems such as wind turbines, compressors, and motion platforms [18], while the identification of LTV joint admittance has received less attention.

In LTV human experiments there are four main limitations:

- 1) It is not possible to have full control on the dynamics of the time variation [26].
- 2) There is a high level of noise in the system [45].
- 3) The experimental time is limited.
- 4) There is limited *a priori* knowledge on the system dynamics.

Previous studies on the identification of LTV human joint admittance neglected at least one of these limitations. In [16], [17], [28] the ankle of the subjects was attached to a rotational manipulator, which applied position disturbances while the subjects were requested to change their torque with a predetermined pattern. Multiple repetitions of the same condition, with the same determined pattern for the torque, were obtained. With a procedure known as *ensemble averaging*, the time-varying IRF was calculated by averaging over the repetitions. It was assumed that each repetition was collected under the same time-varying conditions, neglecting the first limitation. In [21], [26] the first limitation was neglected as well; both studies applied nonparametric estimation and required the application of ensemble averaging. In [21], the averaging was performed over data collected on a motion platform, while in [26] the collection was obtained during large range motions of the knee joint. In [17], [28], a second-order linear model was fit to the IRF to obtain a parametric model. Similarly, a parametric identification with a fixed model was applied in [4], [40]. The mentioned studies neglect the fourth limitation.

A promising LTV method in the literature that is compatible with the first and fourth limitations is the *Skirt Decomposition method* [18]. The method applies nonparametric identification procedures to retrieve the FRF of a LTV system. The main advantages of the method are that it employs nonparametric techniques, does not require ensemble averaging, and makes no assumptions on the system dynamics. Nevertheless, it makes different assumptions, such as the fact that the time variation should be smooth and slow. The *Skirt Decomposition* has been successfully applied to the identification of LTV electric circuits, yet it is not clear how well it would perform on LTV joint admittance.

Transferring the identification procedures from inanimate objects to humans can be challenging, in particular since human behavior is less predictable and less repetitive, leading to high variability within the system. Furthermore, other intrinsic differences are present that might hinder the applicability of the *Skirt Decomposition* method on joint admittance. First of all, electric circuits operate on a much wider bandwidth than joint admittance does. Secondly, electric circuits are modular systems, in which it is explicit how the time-variation enters the system and how to describe it. Finally, the Signal-to-Noise ratio (SNR) of the considered electric circuits (around 80 dB [19]) is higher than for joint admittance (around 18 dB in [45]).

C. Thesis objective

Two main limitations of the application of LTV methods on the identification of LTV human joint admittance are the lack of control of the dynamics of the time variation and the limited *a priori* knowledge on the system dynamics. In literature, attempts have been made to identify LTV human joint admittance; however, the methods neglected either one of the two limitations. The fundamental motivation of this study is to tackle both limitations by utilizing a LTV method that requires neither the repeatability of the time variation nor a parametrization of the system's dynamics. Although the proposed method has been already utilized on electric LTV systems, its application on the identification of LTV human joint admittance is completely novel.

First, the selected method is explained in order to provide the readers with the background required to understand the remaining of the paper and to present the employed notation. Secondly, a simplified model of LTV human joint admittance is introduced. The model is used in simulations to validate the method on a system with dynamics similar to those of LTV human joint admittance. The results from the simulation are discussed to gain understanding on the effects that different parameters have on the identification of the model. Thirdly, the method is applied on human data obtained experimentally from the wrist joint. The results are analyzed and compared with the simulation results. Finally, the benefits of the application of the selected method on the identification of LTV human joint admittance are discussed and conclusions are drawn.

II. SKIRT DECOMPOSITION METHOD

A. Modeling of LTV systems

The dynamics of a linear slowly time-varying system can be represented by its system function: a 3-dimensional mapping which expresses how the frequency-domain properties of the system evolve over time (Appendix B, [20]). The system function can be modeled as the series expansion of LTI components $G_p(j\omega)$ multiplied by user-defined basis functions $b_p(t)$, ($p = 0, 1, \dots, N_p - 1$). When an arbitrary input is applied to the system, each "branch" of the series expansion affects the input separately, and the overall response of the system is determined by the sum of the outputs of each branch (Figure

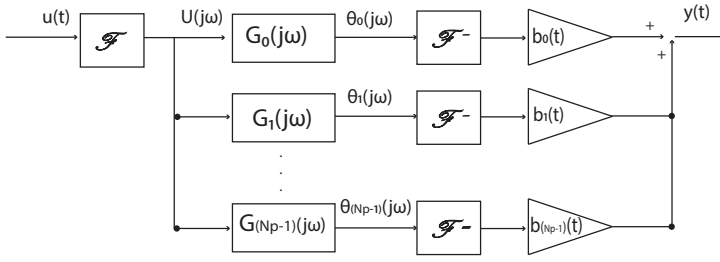


Figure 1: Decomposition of the input $u(t)$ into N_p branches. In each branch, the input in the frequency domain is multiplied by a LTI component $G_p(j\omega)$, and the resulting signal is multiplied in the time domain by a basis function $b_p(t)$. The sum of each branch determines the output $y(t)$.

1). The steady-state output can be expressed as:

$$y_{ss}(t) = \sum_{p=0}^{N_p-1} [\mathcal{F}^{-1}(\theta_p(j\omega))b_p(t)] \quad (1)$$

where:

- y_{ss} is the steady-state output in the time domain;
- \mathcal{F}^{-1} is the inverse Fourier transform operator;
- $U(j\omega)$ is the input in the Fourier domain;
- $\theta_p(j\omega) = \frac{1}{2\pi}(G_p(j\omega)U(j\omega))$.

In each branch of the equation, $\mathcal{F}^{-1}(\theta_p(j\omega))$ represents a LTI response in the time domain which gets multiplied by a basis function in time. If the same expression is reported to the frequency domain, the multiplication to the basis function $b_p(t)$ becomes a convolution to $B_p(j\omega)$, the equivalent in the frequency domain:

$$Y_{ss}(j\omega) = \sum_{p=0}^{N_p-1} [\theta_p(j\omega) * B_p(j\omega)] \quad (2)$$

If the input applied to the LTV system is a multisine, i.e. a signal composed of the sum of sinusoids with different frequencies, then the output spectrum presents peaks at the excitation frequencies but also power at the non-excited frequencies. The shape of the amplitude spectrum results in the repetition of peaks and valleys; the portion of the spectrum between two valleys is defined as a "Skirt".

The presence of the Skirts in the output spectrum is related to the time variation in the system. In Figure 2, it is explained how Skirts appear in the output spectrum when a multisine input is applied to one branch of Equation 2. The LTI response $\theta_p(j\omega)$ of a multisine signal presents peaks at the excitation frequencies only. Since the Fourier transform of the basis function $b_p(t)$ is typically a Skirt centered at the origin, when $B_p(j\omega)$ is convolved with $\theta_p(j\omega)$, the output spectrum results into multiple Skirts centered at each excitation frequency.

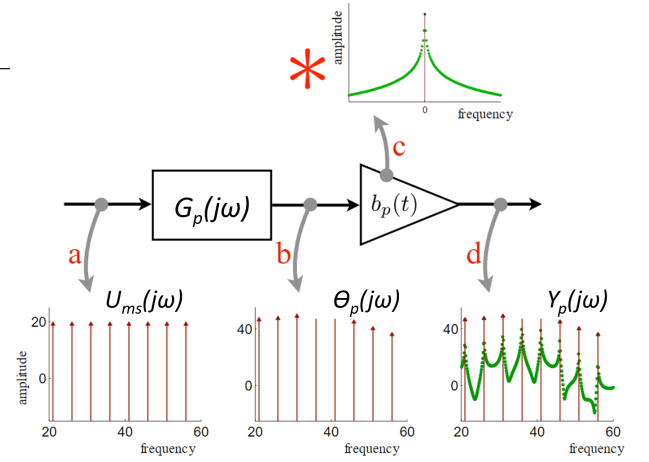


Figure 2: Steps representing Equation 2 for a single branch and a fixed N_p . **a.** The spectrum of a multisine input presents peaks only at the excited frequencies. **b.** For a multisine input through a LTI system, the output spectrum contains peaks at the frequencies contained in the input. The magnitude of each peak depends on the LTI transfer function that shaped it. **c.** The frequency spectrum of a slow and smooth basis function is typically shaped like a Skirt of variable width. **d.** The output spectrum of a LTV system is the convolution of the Skirt with the LTI output spectrum. (Picture edited from [3])

B. Main identification steps

The *Skirt Decomposition* method is a nonparametric SI approach which fits predetermined functions onto the frequency spectra of a LTV system. The aim of the method is to reconstruct the LTV system function. The *Skirt Decomposition* method is formulated assuming that the time variation of the target system can be represented in the frequency domain by smooth decaying functions with power concentrated at low frequencies (Assumption 1). The assumption is equivalent to stating that the time variation of the target system is slow and smooth [20]. Under Assumption 1, $B_p(j\omega)$ are Skirts centered at the origin and the output spectrum is composed by the repetition of Skirts (Figure 2.d).

It is possible to discern the contribution of each Skirt by using linear least-squares regression on the measured output signal and the predetermined basis functions [20]. For the application of the linear least-squares regression, the expression in Equation 2 is rewritten in matrix form in function of the discrete frequencies $j\omega_k$. To reduce the computational time, it is assumed that at each non-excited frequencies the power of the output is determined by the time variation of the three closest excitation frequencies (Assumption 2). The contribution of the neglected excitation frequencies is modeled as a smooth polynomial of order N_{tr} in function of the discrete frequencies $j\omega_k$ (Appendix C). The smooth polynomial also captures the transient dynamics, and the coefficients are estimated in least-squares regression together with the LTI coefficients. For notational simplicity, the matrix multiplication

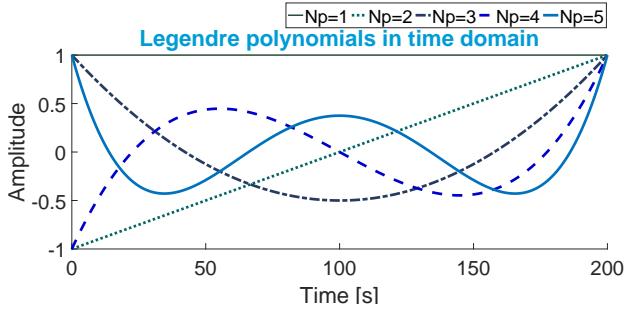


Figure 3: Representation of the first five Legendre Polynomials in time.

can be written as:

$$Y(j\omega_k) = B(j\omega_k)\Theta(j\omega_{ke}) \quad (3)$$

in which $B(j\omega_k)$ contains the Fourier transform of the relevant basis functions and different powers of $j\omega_k$, while the vector $\Theta(j\omega_{ke})$ contains the LTI responses $\theta_p(j\omega_{ke})$ and the coefficients of the smooth polynomial. The LTI responses are non-zero at the excitation frequencies only. $\Theta(j\omega_{ke})$ is estimated using linear least-squares regression (Appendix C-C). It is assumed that the matrix $B(j\omega_k)$ is nonsingular and invertible (Assumption 3). From the vector $\Theta(j\omega_{ke})$ and the basis functions $b_p(t)$, the output in the time domain and the system function can be reconstructed.

III. SIMULATION STUDY

A. Simulation method

1) Simulink model

A mass-spring-damper model with the stiffness varying in time was implemented in Simulink (The Mathworks inc.) to represent LTV joint admittance. The dynamics of the model are represented by the following equation:

$$I_c \frac{d^2\theta(t)}{dt^2} = [T(t) - B_c \frac{d\theta(t)}{dt} - K(t)\theta(t)] \quad (4)$$

In Equation 4, the imposed torque $T(t)$ and the angular position $\theta(t)$ are the input and output of the system, respectively. The scalars I_c and B_c are the inertia and viscosity constants, while the function $K(t)$ represents the changing stiffness. The transfer function representing the system in Laplace domain is:

$$\frac{\Theta(s)}{T(s)} = \frac{1}{I_c s^2 + B_c s + K(t)} \quad (5)$$

in which s is the Laplace variable, and $\Theta(s)$ and $T(s)$ are the input and the output in the Laplace domain. Zero-mean white noise was added to the output.

In LTI conditions, it is common practice to represent joint admittance with a linear mass-spring-damper model [9], [27], [38]. The time variation was introduced by imposing a change of stiffness in time, following the structure used in [26].

Table I: Model and identification parameters varied in the four case studies.

Case study	Δf_{exc} [Hz]	Stiffness [$\frac{Nm}{rad}$]			Np
		Function	K_{min}	K_{max}	
1:	0.2, 0.8, 1.4	Linear	0.5	6	1,2,...,20
2:	0.2, 0.8, 1.4	Reciprocal of a linear function	0.4	6	1,2,...,20
3:	0.2, 0.8, 1.4	Sinusoidal	0.5	6	1,2,...,20
4:	0.8	Linear	1/6	0.2, 4.2,...,12.2	1,2,...,20

2) Model and identification parameters

Three key design parameters were varied within the simulation and their combined effect on the accuracy of the *Skirt Decomposition* method was analyzed over four case studies. The first parameter is the distance between the excitation frequencies in the multisine signal. The distance between consequent excitation frequency was kept constant and expressed with Δf_{exc} (Hz). The design of Δf_{exc} has an influence on both the frequency resolution and the distance between the Skirts in the output spectrum. The second parameter which was varied is N_p , representing the number of basis functions employed. The parameter influences the shape of the predetermined Skirts used to fit the output spectrum. The last parameter is $K(t)$, representing the change of stiffness in time. The complexity and the rate of change of the stiffness were changed in the case studies, with effects on the shape of the Skirts in the output spectrum. The stiffness $K(t)$ was defined in terms of the mathematical function representing it, the minimal amplitude (K_{min}) and the maximal amplitude (K_{max}). To vary the complexity of the time variation, mathematical functions with different smoothness were used. To vary the rate of change of the time variation, the maximal amplitude was varied, while the minimal amplitude was kept invariant. The values for Δf_{exc} , N_p and $K(t)$ tested over the four case studies are summarized in Table I. The relevance of a proper design of Δf_{exc} and the basis functions with respect to the time variation is reinforced by the limited bandwidth of the system when compared to that of electric circuits. The number of frequency points available is constrained by the bandwidth of the system, limiting the options for Δf_{exc} .

The other simulation parameters were kept constant and are summarized in Table II. The inertia and damping of the model are representative of the dynamics of wrist admittance [37]. The basis functions utilized are the Legendre polynomials (Figure 3), which have been shown to provide a good approximation of arbitrary time variation [20]. The multisine signal was defined over a period T_m of 10 seconds. The simulation time lasted 200 seconds, hence the multisine was repeated 20 times to generate the perturbation signal.

3) Performance analysis

For every combination of the tested model parameters, the simulation was run twice. In this manner, two data sets were obtained which were successively divided into a test and a

Table II: Model and identification parameters considered as constant in the Simulation, including the notation used, a brief description and the units.

Name	Description	Value	Unit
A_{max}	Max Amplitude multisine signal	1.5	[Nm]
B_c	Damping	0.05	$[\frac{Nm\cdot s}{rad}]$
$b_p(t)$	Basis functions	Legendre pol.	[]
f_{exc1}	Smallest excitation frequency	$\frac{1}{T_m}$	[Hz]
f_{excM}	Highest excitation frequency	20	[Hz]
fs	Sample frequency	200	[Hz]
I_c	Inertia	0.02	$[\frac{Nm\cdot s^2}{rad}]$
N_{tr}	Order Transient polynomial	3	[-]
SNR	Signal-to-noise ratio of the output signal	20	[dB]
T_m	Period of the multisine signal	10	[s]
T_{sim}	Length of the simulation	200	[s]

validation dataset. The test dataset was used to build a model of the system. The input from the validation dataset was applied to the model to obtain an estimate of the output (Appendix C-E). The accuracy of the estimation is expressed in form of the Variance Accounted For (VAF) between the noiseless, measured output and the estimated output of the validation dataset. The expression of the VAF is:

$$VAF = \max \left\{ 1 - \frac{\text{var}(y(t_k) - \hat{y}(t_k))}{\text{var}(y(t_k))}, 0 \right\} \cdot 100\% \quad (6)$$

Another indicator that was used to determine the goodness of fit is the Root-Mean-Square-Error (RMSE) between the estimated resonance frequency and the real resonance frequency of the model in time. The estimated resonance frequency was extracted from the retrieved system function, while the system resonance frequency was obtained by solving $f_n = \frac{1}{2\pi} \sqrt{\frac{K(t)}{I_c}}$.

B. Simulation results

1) Case studies 1,2,3

The estimation accuracy of case studies 1, 2 and 3 is depicted in Figure 5. The accuracy was expressed in terms of the VAF and RMSE of the resonance frequency in timw. In the first row, the VAF for different combinations of Δf_{exc} and number of basis functions are shown. For the three case studies, a common trend can be recognized: regardless of Δf_{exc} , the VAF for $N_p = 1$ started at a minimum value and it increased progressively with the order of the Legendre polynomial, reaching a maximum threshold around 100%. On the other hand, if a small Δf_{exc} ($\Delta f_{exc} = 0.2$ Hz) was combined with a large N_p ($N_p \geq 14/T_m$) then the VAF was reduced, dropping up to 0%. A similar trend can be recognized in the second row, where the RMSE is plotted. The increment of N_p decreased the estimation error; nevertheless, if a large N_p was combined with a small Δf_{exc} the error started increasing.

Despite the common trend, the performance assumed different numerical values depending on the shape of the stiffness

imposed in the case study. It can be seen that for $N_p = 1$, the VAF relative to *case study 3* (sinusoidal stiffness) was around 30%, while the VAF relative to *case study 2* (reciprocal stiffness) was about twice as big. The VAF assumed an intermediate value of around 40% in *case study 2* (linear stiffness). Furthermore, in *case study 1* the maximum threshold of the VAF was reached for $N_p = 10$, in *case study 2* for $N_p = 6$ and in *case study 3* for $N_p = 16$. The value for Δf_{exc} had a visible effect on the RMSE of *case study 1*: for Δf_{exc} of 0.2 Hz the RMSE reached a minimum around 0.1 Hz, while for Δf_{exc} of 1.4 Hz it reached a minimum around 0.5 Hz. Finally, it can be seen that for every case study, there existed at least one combination of N_p and Δf_{exc} that corresponded to a VAF higher than 90% and a RMSE lower than 0.1 Hz.

In Figure 6, the condition number of the regression matrix $B(j\omega_k)$ (Equation 3) is shown for different choices of N_p and for different values of Δf_{exc} . The figure shows a positive correlation between the number of basis functions N_p and the condition number. For $N_p = 1$, the condition number was equal to 1, regardless of the value of Δf_{exc} used in the input. The condition number grew by increasing N_p and the growth was faster for smaller Δf_{exc} . The condition number reflects the significant figures that can be lost in accuracy due to inversion. The higher the condition number, the closer the matrix to being ill-conditioned. For example, the plot indicates that for $N_p = 20$ and Δf_{exc} of 0.2 Hz there can be a loss of accuracy of almost 5 significant digits.

2) Case study 4

A case study with a varying rate of change of the stiffness was performed. The purpose of this investigation was to quantify the assumption on the speed of time variation. To introduce a gradually increase of the time variation, the identification accuracy was tested for multiple values of K_{max} , proportional to the rate of change of the stiffness function. In Figure 7, the results from Case study 4 are depicted. The figure shows the estimation accuracy obtained by varying the maximum amplitude of the stiffness K_{max} and the number of basis functions N_p . The plot shows that the estimation accuracy, indicated by the VAF and the RMSE on the estimated stiffness, decreased with an increase of the rate of change of the stiffness function. When K_{max} was set to 0.2 Nm/rad the VAF was around 100 % and the RMSE of the resonance frequency was around 0.15 Hz. Instead when K_{max} was set to 12.2 Nm/rad the VAF ranged between 20 % and 90 % and the RMSE ranged between 0.25 Hz and 2.5 Hz. Generically, the accuracy increased with the value of N_p .

C. Discussion on simulation study

1) Effects of design parameters on simulation accuracy

a) Number of basis functions.

The number of basis functions employed in the *Skirt Decomposition* method was varied in the four case studies. In Figures 5 and 7, a general proportionality between the number of basis functions N_p and the performance was pointed out. The beneficial contribution that N_p has on the estimation accuracy can be related to the fact that a higher number of branches is used for identification. In other words, more basis functions are

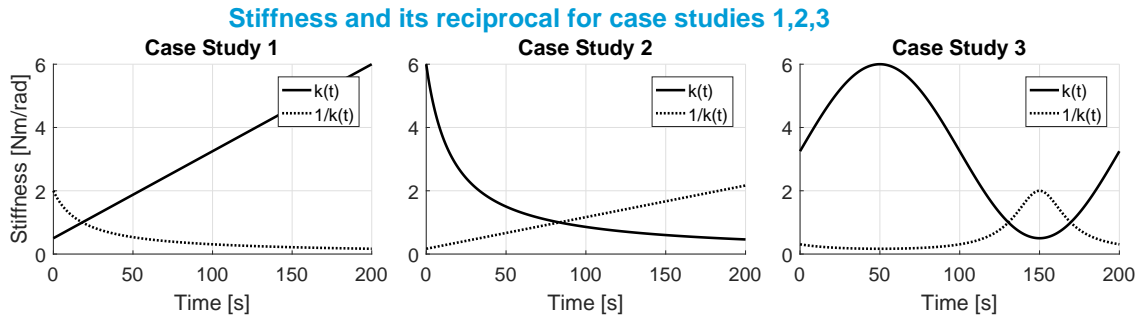


Figure 4: Representation of the stiffness used in the three different case studies. The continuous black line represents the stiffness, while the dotted line represents the reciprocal of the stiffness.

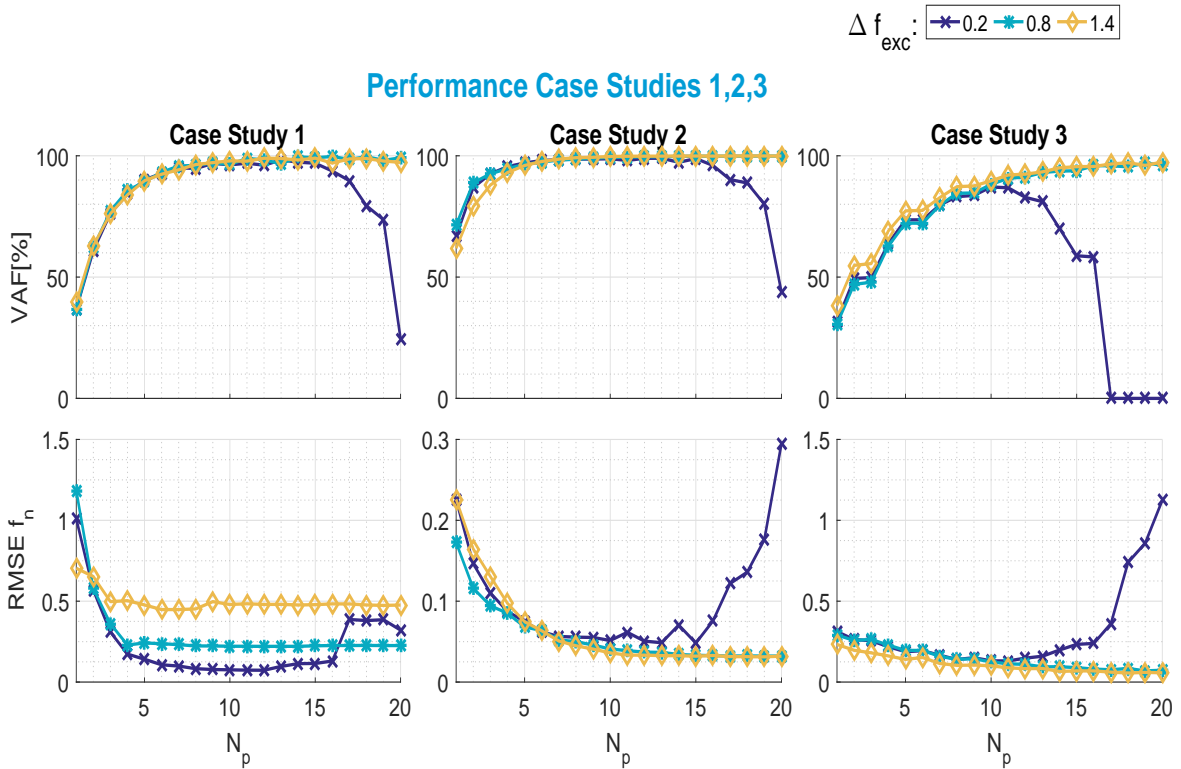


Figure 5: Performance of the simulation on a validation dataset for *case studies* 1, 2 and 3. The figure represents the results for several, distinguished identification procedures. Each result is labeled with a marker, which was obtained through a SI procedure with a different value for N_p and Δf_{exc} . All the remaining parameters are kept the same. Markers of the same type and color correspond to an identification performed by using the same value for the Δf_{exc} . The markers are interconnected by a line of the same color for graphical clarity. The horizontal axis represents N_p , the number of Legendre polynomials used for the identification. The calculations are done for N_p ranging from 1 to 20 and for Δf_{exc} from 0.2 Hz to 1.4 Hz. In the first row, the vertical axis represents the VAF between the estimated output and the noiseless output on a validation set. In the second row, the vertical axis represents the RMSE between the imposed stiffness and the calculated stiffness on the same validation set.

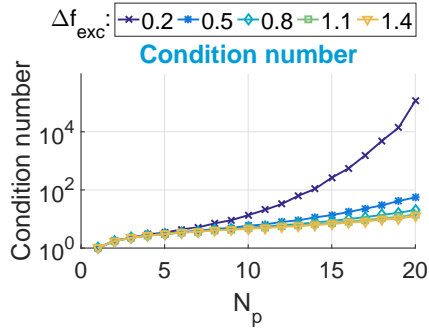


Figure 6: Condition regression number of the matrix $B(j\omega_k)$ (Equation 3) for varying Δf_{exc} and number of basis functions. The values for Δf_{exc} range between 0.2 Hz and 1.4 Hz, while the values for N_p range between 1 and 20.

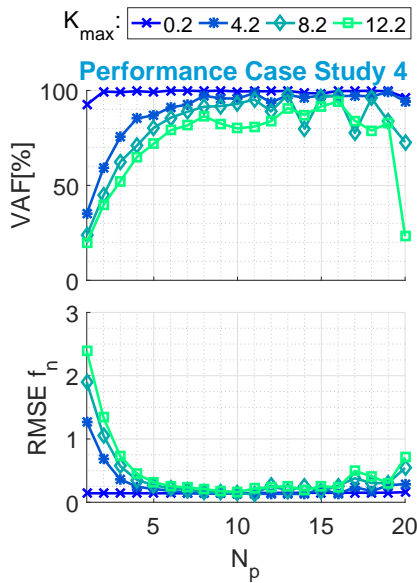


Figure 7: Performance on a validation dataset for *case study 4*. The horizontal axis is defined by the rate of change of the time variation, expressed by K_{max} , while the vertical axis represents the VAF between the noiseless output and the estimated output (first row) and the RMSE between the estimated resonance frequency and the system's resonance frequency Hz (second row). The plot is obtained for K_{max} ranging from 0.2 to 12.2 Nm/rad , for Δf_{exc} of 0.8 Hz and for N_p ranging from 1 to 20.

employed in the procedure, enhancing the Degrees of Freedom (DOF) for the approximation. It follows that increasing N_p generally enhances the approximation power of the *Skirt Decomposition* method.

b) Complexity of the time variation.

The complexity of the imposed stiffness was changed between case studies 1, 2 and 3 and the results are presented in Figure 5. To understand the outcomes of the identification, it

is important to keep in mind a key concept: in the simulation, the time variation is inversely proportional to the value of the stiffness. In fact, $K(t)$ guides the time-varying properties into the system although its effect is shaped by the system dynamics. According to the transfer function in Equation 5, the stiffness appears in the denominator, rendering the time variation inversely proportional to it. In particular, it can be deduced that the DC gain, obtained for $s=0$ Hz, is exactly equal to $1/K(t)$. The stiffness imposed in the case studies was designed to result into different levels of complexity of the time variation. Since in *case study 2* the stiffness was defined as the reciprocal of a linear function, the resulting time variation was a linear function. The case study has the lowest complexity of the time variation among the tested ones, as it can be confirmed by looking at the dotted lines in Figure 4. The design choice reflects in the estimation accuracy. In fact, it was seen in Figure 5 that for low values of N_p the performance of *case study 2* was the highest. It can be deduced that the optimal number of basis function for the *Skirt Decomposition* method increases with the complexity of the time variation. The result can be explained by the fact that the Skirts in the output spectra are wider for higher complexity time variations. Therefore, the number of Legendre polynomials required to approximate the output spectrum increases.

c) Speed of the time variation.

Case study 4 was performed to give a representation of the effects that an increase of time variation has on the accuracy of the method. The results depicted in Figure 7 showed an expected trend: an increase in the rate of change in the stiffness resulted in a poorer performance. The trend is related to Assumption 3. When the rate of change of the time variation increases, the power of its spectra gets more spread throughout the frequencies, losing the Skirt-like shape. However, also in this case the performance could be enhanced by employing a higher number of basis functions.

d) Condition number.

The results in Figure 6, reporting an increase of the condition number with the model order, were predictable. The Skirts of higher order polynomials are wider than lower order polynomials, whilst a small Δf_{exc} limits the bandwidth in which each Skirt is expressed. When a small Δf_{exc} is utilized in combination with a large N_p , the Skirts become less distinguishable from each other, entailing a decrease in the apparent order of the matrix $B(k)$. The consequence is a loss of accuracy due to inversion. The loss of accuracy reflects on the identification results. For example, it was seen that for $N_p = 20$ and $\Delta f_{exc}=0.2$ Hz the loss of accuracy due to inversion could be up to 5 significant digits. In Figure 5, the accuracy for the same combination of parameters was minimal.

e) Δf_{exc} .

In all the case studies, multiple values for Δf_{exc} were used. From Figure 5, it can be extracted that the effects of Δf_{exc} on the identification accuracy are related to the order of the Legendre polynomial used for the identification. In particular, it was seen that a large N_p cannot be combined with a small Δf_{exc} . The incompatibility can be partially attributed to the increase of the condition number for this combination of parameters. The presence of noise is an additional cause.

When Δf_{exc} is small, there are not enough data points to discern the smooth contribution of the output spectra from the random contribution of noise. On top of this, if two excitation frequencies are too close to each other, there might be an overlap of the contribution of the relative Skirts onto the neighboring frequencies. Discerning the individual Skirts can become more challenging. It was seen as well that a larger Δf_{exc} is necessary when there is an increase of either the complexity or the speed of the time variation. However, as it was shown in Figure 5 for *case study 1*, a large Δf_{exc} can visibly reduce the accuracy in the approximation of the system function. In fact, having excitation frequencies further away reduces the frequency resolution and the number of points in which the system function is calculated.

D. Sub-conclusions on the simulation study

From the Simulation study, it can be concluded that the *Skirt Decomposition* method can be used to identify a LTV system with dynamics similar to those of joint admittance. However, the application of the method requires a careful choice of the parameters, especially when either the complexity or the speed of the time variation is high. To allow the approximation of Skirts with a larger bandwidth, the number of basis functions should be kept high; nevertheless, the maximum number of basis functions is constrained by the detections of Skirts in the output spectrum. From a computational time perspective, there are no restrictions on the order of the basis functions, since the *Skirt Decomposition* method uses simple algebraical tools on a limited set of points (Assumption 2). Furthermore, it was seen that a high N_p increases the approximation power of the method. On the other hand, Δf_{exc} should be increased accordingly to N_p to allow the formation of Skirts in the output spectra and to prevent an increase of the condition number. When the excited frequencies are too far apart, the frequency resolution drops and the properties of the system cannot be approximated accurately. It follows that a trade-off between the order of the basis functions and the excitation frequencies design should be found. In the simulation study, it was possible to find the right combination of N_p and Δf_{exc} to obtain a VAF approaching 100% and a RMSE of the resonance frequency lower than $0.1Hz$ for each one of the tested time variations.

IV. EXPERIMENTAL STUDY

A. Experimental method

1) Subjects

Three young healthy subjects, two males and one female, participated in the pilot experiment. The subjects are denoted in the paper by the Roman numerals I, II and III.

2) Setup

The experimental apparatus that was used in the pilot study is the *PoPe*, a one degree-of-freedom robotic wrist manipulator [37], [46]. The right forearm of the subjects was strapped into an armrest secured to the device. The axes of rotation of the manipulator and the wrist were aligned, allowing only for flexion and extension of the wrist on the horizontal plane. The subjects interacted with the manipulator via a handle and

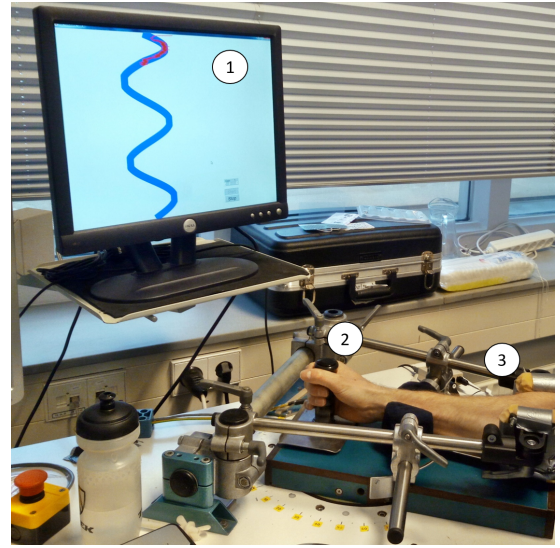


Figure 8: Picture of the PoPe setup. 1: Screen, showing the desired torque trajectory in blue, allowing for a error of around $\pm 2\%$, and the applied torque in red. 2: Handle of the manipulator. 3: Armrest around the forearm of the subject.

were asked to hold it firmly with their right hand (Figure 8). The device was configured as a stiff position servo, and the angular position of the handle was imposed to the wrist. The torque applied by the subjects on the handle was measured by the device, together with the angular position of the wrist. The signals were measured with a sampling frequency of $2.5kHz$ and a 16-bins resolution. Electrical and mechanical safety stops were preventing harmful flexion/extension of the handle beyond the wrist' range of motion.

The subjects were seated in front of a screen, displaying a low-passed version of the exerted torque (cut-off frequency of 1 Hz) and a trajectory in time, expressing a desired torque level. The subjects were instructed to vary the applied torque to track the desired trajectory, minimizing torque deviations. The margins of the desired torque trajectory were increased to allow for an error between the desired trajectory and the measured torque around $\pm 2\%$. The subjects were requested to use only the flexor muscles to perform the task.

3) Task

At the beginning of the experiment, a preliminary measurement was performed. In this preliminary step, the subjects were asked to flex the wrist to a maximal level. The maximum torque applied was used to determine the subject-specific Maximum Voluntary Contraction (MVC), necessary for the design of the desired torque trajectory. The minimal and the maximal amplitude of the desired trajectories were indeed expressed in the form of a percentage of the measured MVC.

In the main experiment, four different conditions were tested, varying among each other for the shape of the desired torque trajectory. Each trajectory was composed by the signal of interest and a transitory part. The transitory part was required by the controller and was necessary to allow the

subjects to adjust to the tasks. For each trial, the transitory part lasted for a total of 10 s.

The conditions tested were the following:

- *Sawtooth Condition*: The signal of interest was represented by two consequent ramps of equal length $T_{ramp} = 40$ s. Zero-gradient transitory parts were added before the first ramp (4.4 s), in between the ramps (4.5 s), and after the second ramp (0.1 s). The trajectory lasted for 90 s.
- *Slow Sine Condition*: The signal of interest comprised two repetitions of a sine with a period of 40 s and no phase shift. A complementary part of 9.9 s, composed by half period of a sinusoid, was added before the sine and a zero-gradient part of 0.1 s afterward. The trajectory lasted 90 s.
- *Intermediate Sine Condition*: The shape was similar to that of the slow sine condition, although the period of the sine was of 30 s. The trajectory lasted for 70 s.
- *Rapid Sine Condition*: The signal of interest was composed by four repetitions of a sine with a period of 20 s. The complementary part was the same as for the slow and intermediate sine conditions. The trajectory lasted for 90 s.

Finally, a *Relax Condition* was considered. The subjects were asked to relax the muscles without reacting to the perturbations. The condition represented a LTI case [43] and it lasted for 70 s.

For each condition, 3 trials of equal length were recorded. The observation time of the trials was adjusted to the length of the desired trajectory. The trials were presented in random order to the subjects. Subject I and II performed trials for the relax and intermediate sine conditions, while subject III performed trials for the relax, slow sine, intermediate sine, and sawtooth conditions.

The percentage of the MVC that defined the minimal and maximal amplitude of the desired torque trajectory was also varied between subjects. For subjects I and II, the amplitude ranged between 10% and 50% of the MVC, for subject III it ranged between 5% and 20%. A summary of the conditions and specification for the three subjects is provided in Table III, while a visual representation of the sawtooth, fast sine and slow sine conditions applied on subject III is given in Figure 9.

4) Perturbation design

The perturbation input comprised a sequence of multiple realizations of the same multisine signal, each with a period of 10 s. The input excited frequencies ranging from 0.1 Hz to 20.0 Hz, with a fixed distance Δf_{exc} of 0.8 Hz. The value of Δf_{exc} selected provided a good trade-off in the simulation study. The power at the excited frequencies was equal until 6 Hz and decreased afterward of $20\text{dB}/\text{decade}$, following the indications in [45]. The imposed angular perturbation was designed to generate an RMS wrist angular excursion of 0.02 rad [46].

The multisine perturbation was applied in correspondence to the signal of interest. For the transitory part, a supplementary perturbation was implemented to guarantee a continuity of the perturbation throughout the trials. The supplementary

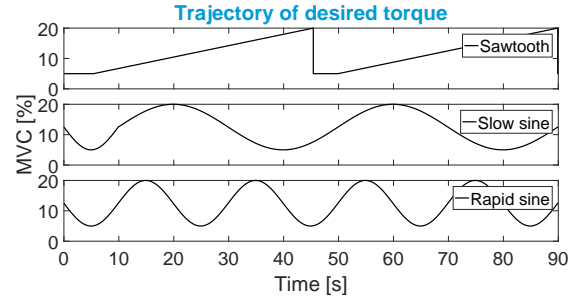


Figure 9: Representation of the trajectories for the desired torque for the conditions tested on subject III. (The relax condition was tested as well, but is not represented.)

perturbation was essentially a shorter reproduction of the primary multisine perturbation. The portion of the input and output signals that was measured during the transitory part was discarded from the analyzed data.

5) Pre-processing of the data

In this paper, the measured output is considered as the sum of two signals, $y_v(t)$ and $y_\theta(t)$ (Figure 10). The voluntary output $y_v(t)$ is the torque which is applied by the subject to track the desired torque trajectory. The signal $y_\theta(t)$ represents the output of the system in response to the application of the perturbation signal $\theta(t)$. The time-varying behavior of the joint dynamics is expected to be triggered by $y_v(t)$. On the other hand, the signal that is of interest for the application of the *Skirt Decomposition* method is solely $y_\theta(t)$. To obtain a representation of the signal $y_\theta(t)$, an estimate of the voluntary torque $y_v(t)$ was subtracted from the measured output. It was assumed that there was a linear relationship between the voluntary torque $y_v(t)$ and the desired torque trajectory $y_v^*(t)$. Therefore, the measured output was expressed as in Equation 7.1. The constant a was retrieved by solving linear least-squares between the measured output and the desired torque trajectory (Equation 7.2). The multiplication between the constant a and the desired torque trajectory was then subtracted from the measured output, providing an estimate of $y_\theta(t)$ (Equation 7.3).

1. $y_m(t) = y_\theta(t) + a \cdot y_v^*(t)$
2. $\hat{a} = \min_a \|y_m(t) - y_v^*(t)\|_2^2$ (7)
3. $\hat{y}_\theta = y_m(t) - \hat{a} \cdot y_v^*(t)$

The second step of the pre-processing was to subtract the mean of the input and the output to remove the DC gain. Finally, the signals from each trial were divided into segments of equal length. The partition was performed ensuring that the duration of each segment was an integer multiple of the period of the multisine signal. For the relax condition, a segment lasted for 60 s. For the sawtooth conditions, the segments had the same duration of a single ramp, while for the sinusoidal conditions, each segment was equal to the period of the sine. Finally, for the slow sine condition, segments equal to half the period of a sine were considered as well. The segments are

Table III: Summary of the specifications for the different conditions tested. The first column expresses the shape of the torque trajectory used. The second column expresses the observation time. The third column the minimum and maximum torque level of the desired trajectory, expressed in terms of percentage of the MVC. The fourth column expresses the subjects on which the condition is tested. The last column reports additional specifications on the duration of the signals of interest.

Torque Trajectory	Observation time [s]	Min.- Max. Torque [%MVC]	Subjects	Additional Specifications
Relax	70	10-50	I, II, III	None
Slow Sine	90	5-20	III	period= 40 [s]
Intermediate Sine	70	10-50	I, II	period= 30 [s]
Rapid Sine	90	5-20	III	period= 20 [s]
Sawtooth	90	5-20	III	$T_{ramp} : 40$ [s]

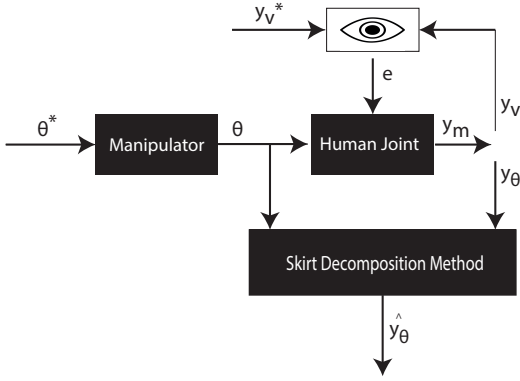


Figure 10: Block diagram of the setup. The subject is requested to follow a desired trajectory, and receives visual feedback on the applied torque and on the desired torque level y_v^* . To track the desired torque trajectory, the subject changes the value of joint admittance. On top of this, the manipulator applies a small range angular perturbation θ to the joint. The effects that the perturbation have on the applied torque y_θ is dependent on joint admittance, which is changed by the tracking task. The overall measured output y_m is composed by the signals y_θ and y_v . The signal θ and y_θ are used as input and output signals for the application of the *Skirt Decomposition* method. An estimate \hat{y}_θ of the output is obtained.

labeled with a letter and a subscript number, the first indicating the trial, the second the segment number in the trial.

6) Data and performance analysis

The *Skirt Decomposition* method was applied to the measured angular position (input) and the pre-processed measured torque (output). The accuracy in the time domain was expressed in terms of VAF between the output and the estimated output. In the frequency domain, the accuracy was calculated in terms of residuals. The residuals represent the difference between the absolute values of the measured torque and of the

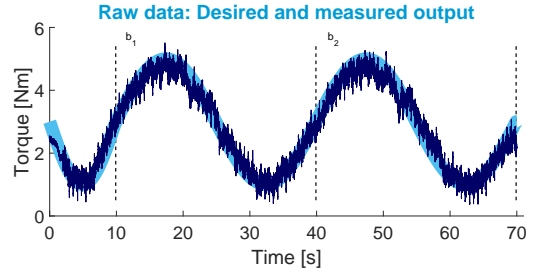


Figure 11: Raw data from subject I, trial b, for an intermediate sine trajectory condition. The light blue line corresponds to the desired torque, with a margin of $\pm 2\%$ and the dark blue corresponds to the torque measured from the subject. The Figure is obtained for an MVC of 10 Nm , and the desired torque ranges from 10% to 50% of the MVC. The dotted lines demarcate the segments used for identification, the letter on top b is used to labeling the trial number, and the subscript indicates the segment number.

estimated torque in the frequency domain. The Root-Mean-Square (RMS) of the residuals in the bandwidth 0.1-20 Hz was calculated. The bandwidth corresponded to the range of frequencies excited by the multisine.

A comparative analysis was performed to assess the effects that the different experimental conditions and identification parameters had on the accuracy of the *Skirt Decomposition* method. The VAF and the RMS residuals were computed for each segment. The segments measured from subjects I and II were analyzed using eight basis functions, while for the segments from subjects III five basis functions were implemented. Furthermore, the segments were analyzed using a $zero^{th}$ order basis function ($N_p = 1$). The $zero^{th}$ order analysis corresponded to an identification performed at the excitation frequencies only. The results were compared to the higher order analysis to assess the contribution of the non-excited frequencies on the accuracy.

The data measured from subjects III were analyzed further in a validation study. For each condition and subject, a random segment was selected and used as test dataset. The remaining segments constituted the validation dataset. The VAF and residuals for the test and validation datasets were computed. The residuals were calculated as well in the bandwidth 2-20 Hz, where the variability of the output was supposed to be lower than for the frequencies until 2 Hz. Successively, the distribution of the residuals over the excited bandwidth on an representative segment was analyzed. Finally, the system function was obtained, and from it, the resonance frequency was extracted.

B. Experimental results

1) Input and output data

An example of the raw data obtained from the experiment is provided in Figure 11. The figure shows the desired and measured torque obtained for the intermediate sine condition on subject I. The dark blue line, representing the torque exerted

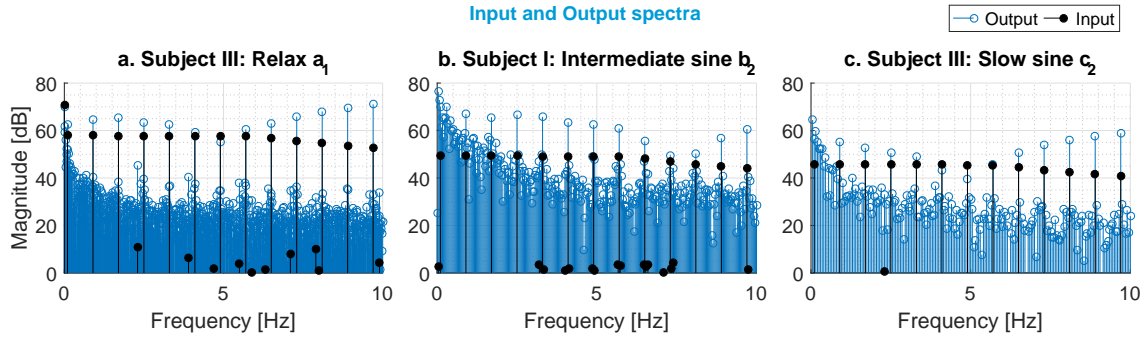


Figure 12: Spectra of the input (black) and output (blue) after pre-processing from different subjects and conditions. Panel a represents the spectra from the relax condition, obtained using segment a_1 from subject III. Panel b represents the spectra from the intermediate sine, obtained using segment b_2 from subject I. In the condition, the desired torque trajectory ranged between 10% and 50% of the MVC. Panel c represents the spectra for the slow sine condition and is obtained using data from segment c_2 (20 s segment) from the slow sine condition. In the condition, the desired torque trajectory ranged between 5% and 20% of the MVC.

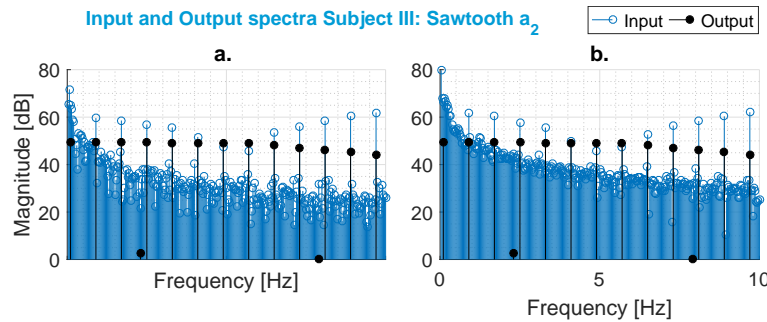


Figure 13: Spectra of the input (black) and output (blue) from the sawtooth condition from subject III, segment a_2 . Panel a represents the spectra after pre-processing. Panel b represents the spectra obtained by using the pre-processed input and the full measured output.

by the subject, is within the desired boundaries throughout the observation time. It can also be observed that the mean trajectory applied by the subject was not a pure sinusoid, and presented some discontinuities.

Figures 12 and 13 show the magnitude of the input and output spectra for different subjects and conditions. In both figures, it is possible to recognize the input spectra, represented in black, the output at the excitation frequencies, corresponding to the peaks in blue, and the output at the non-excited frequencies, corresponding to the blue lines at lower power. Additionally, it can be seen that the power at the non-excited frequencies in the frequency band 0-2 Hz is higher than at the other non-excited frequencies. In Figure 12, the spectra from the relax condition is compared to the spectra from the intermediate sine and the slow sine conditions. The difference in power between the excitation peaks and the non-excited frequencies varied among the conditions. For the relax task (panel a) the difference was about 30 dB at all frequencies, while it decreased for the other conditions. It can be noticed that for the intermediate sine condition (panel b) the peaks at some excitation frequencies

are barely recognizable. The slow sine condition (panel c) represented a midway case; for this condition, the Skirts around the excitation frequencies can be detected. In Figure 13, the spectra for the sawtooth condition using the overall measured output (panel b) is compared to the spectra using only $y_\theta(t)$ (panel a). Comparing the two plots, a difference in the shape of the spectra can be observed. In panel a, the spectra presents typical peaks at the excitation frequencies and a skirt-like decay of power at the neighboring frequencies. In panel b, the spectra presents a high-bandwidth Skirt centered at the origin and with power up to 10 Hz. The high-bandwidth Skirt overshadows the Skirts around the excitation frequencies. Only the peaks at the excitation frequencies remain evident.

2) Estimation accuracy

In Table IV, the mean VAF and RMS residuals for all the tested subjects and conditions are reported, and the number of basis functions utilized for the analysis is mentioned. For subjects I and II, $N_p = 8$ was selected, while the number of basis functions was decreased to 5 for subject III. Additionally, the accuracy obtained by utilizing a $zero^{th}$ order basis function ($N_p = 1$) is reported, and expressed as VAF_0 and RES_0 .

Table IV: Mean and standard deviation of the VAF and the RMS residuals (RES) for different subjects and conditions. The value selected for N_p is displayed in the corresponding column. The length of the individual segments is reported, together with the number of segments over which the averaging is performed. For the slow sine condition, segments of 40 s and 20 s were used. Additionally, the mean and standard deviation of the VAF and the RMS residuals obtained using a $zero^{th}$ order basis function ($N_p = 1$) are reported with the subscript 0.

	Relax	Slow Sine		Intermediate Sine		Rapid Sine	Sawtooth
Subjects(s):	I-II-III	III	III	I	II	III	III
N_p :	1	5	5	8	8	5	5
Length of each segment:	60 s	40 s	20 s	30 s	30 s	20 s	40 s
Tot. N. of segments:	9	6	12	6	4 ^[1]	12	6
VAF [%]:	n.a.	78.2 (8.8)	93.6 (2.8)	81.5 (1.4)	57.4 (9.2)	90.5 (6.2)	86.1 (5.7)
VAF_0 [%]:	95.9 (1.6)	73.3 (9.4)	80.9 (8.8)	61.2 (7.7)	32.5 (7.9)	62.5 (9.6)	76.7 (14.1)
RES :	n.a.	65.0 (10.5)	32.7 (12.6)	170.5 (16.8)	430.8 (112.0)	46.8 (18.0)	87.9 (48.1)
RES_0 :	23.3 (10.9)	113.4 (15.0)	66.6 (14.5)	254.9 (16.0)	640.6 (132)	89.0 (23.7)	164.0 (112.5)
		mean (sd)					

[1]: only two trials were recorded due to a technical problem. n.a.= not available.

Table V: Validation results from segments measured on subject III. The VAF and RMS residual of a randomly chosen segment, representing a test set, are expressed. The residuals are computed in the bandwidth 0.1-20 Hz, and in the bandwidth 2-20 Hz. The random segments obtained for the different conditions are b_1, c_2, a_1, c_1 . The mean VAF and RMS residuals of the other segments, used in validation, are depicted as well. The value in brackets represents the standard deviation. For the analysis, N_p was set to 5.

Test Set	Rapid Sine			Slow Sine						Sawtooth		
	20 s			40 s			20 s			40 s		
	VAF %	RES	RES	VAF%	RES	RES	VAF%	RES	RES	VAF%	RES	RES
	0.1-20 Hz	2-20 Hz		0.1-20 Hz	2-20 Hz		0.1-20 Hz	2-20 Hz		0.1-20 Hz	2-20 Hz	
Test Set	96.3	36.8	6.7	85.2	59.6	13.3	92.9	43.4	7.7	88.7	49.6	8.2
Validation Set <i>mean (sd)</i>	63.9 (14.6)	107.6 (44.5)	18.0 (10.8)	71.0 (8.7)	188.9 (59.3)	27.1 (11.0)	62.8 (12.0)	77.7 (30.8)	16.2 (5.7)	70.1 (11.4)	103.6 (29.9)	17.5 (6.9)

It can be seen that the $zero^{th}$ order VAF_0 was maximum for the relax condition (95.9%), while it decreased for all the other conditions, reaching a minimum for the intermediate sine condition (32.5%). A similar trend is recognized for the $zero^{th}$ order RMS residuals. The value was equal to 23.3 for the relax condition, and reached a maximum around 640 for the intermediate sine condition on subject II. For every condition, the VAF and the RMS residuals calculated using higher order basis functions ($N_p = 5, 8$) resulted in higher accuracy than for the $zero^{th}$ order analysis. From Table IV it can be observed that the performance from the three sinusoidal conditions varied between subjects. The results from subject II show the poorer performance, with a mean VAF of 57.4% and a mean RMS residuals of 430.8. The best performance was obtained for the slow sine condition using 20 s long segments, with a mean VAF of 93.6% and a mean RMS residuals of 32.7. In Table V, the validation results from subject III are depicted. For the different conditions, the mean VAF was between 62.8% and 70.1%, and the mean RMS residuals between 77.7 and 188.9. A net decrease in the RMS residuals can be observed in the bandwidth between 2 Hz and 20 Hz. The minimum RMS residuals equaled 16.2 for the slow sine condition and 20 s segments, while the maximum was 27.1 for the 40 s segments from the slow sine condition.

3) Estimated signals

In Figure 15, the estimated output in the time domain is plotted together with the measured output. The figure was obtained using data from subject III performing a slow sine condition. In the figure, it can be observed that the estimated output overlaps with the measured output. As it can be seen in the magnified window on the top of the figure, the estimated output can track the behavior of the measured signal.

The fit in the frequency domain is given in Figure 15. The residuals ranged from around -45dB to 68 dB. The residuals were the highest at the low frequencies (0-2 Hz) and were the lowest in correspondence to the excitation frequencies. As it can be seen in the magnified window at the top of the figure, the error dropped as well at the frequencies close to the excitation peaks. Here the residuals ranged between -6 dB to 6 dB.

Figure 16 represents the system function, obtained using data from the slow sine condition measured from subject III. By looking at the figure in the magnitude-frequency plane, a common behavior can be recognized regardless of the time instance at which the plane is located. At the origin, the magnitude starts at a high value around 15 dB, then gradually drops until reaching a minimum at a frequency around 5 Hz and increases again until reaching a plateau of around 30 dB at the high frequencies. The phase shows a common trend as well:

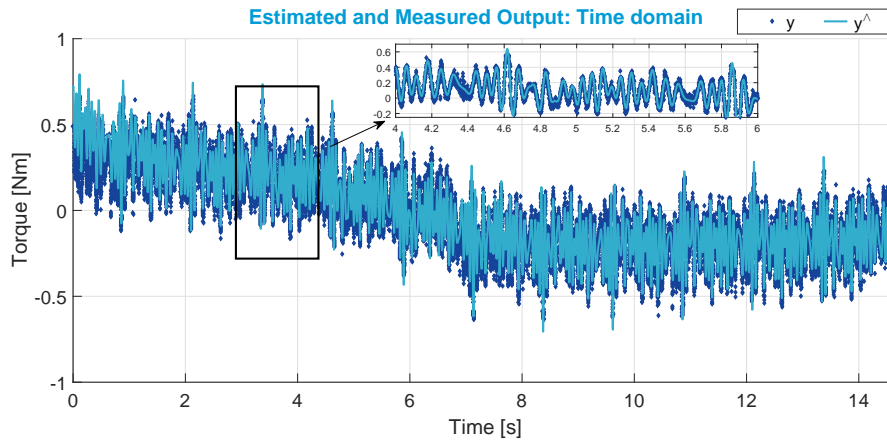


Figure 14: Fit in time domain from subject SIII, Slow Sine condition and segment c_2 . The measured output in time (after pre-processing) is represented by the blue diamonds and the estimated output is represented by the light blue continuous line.

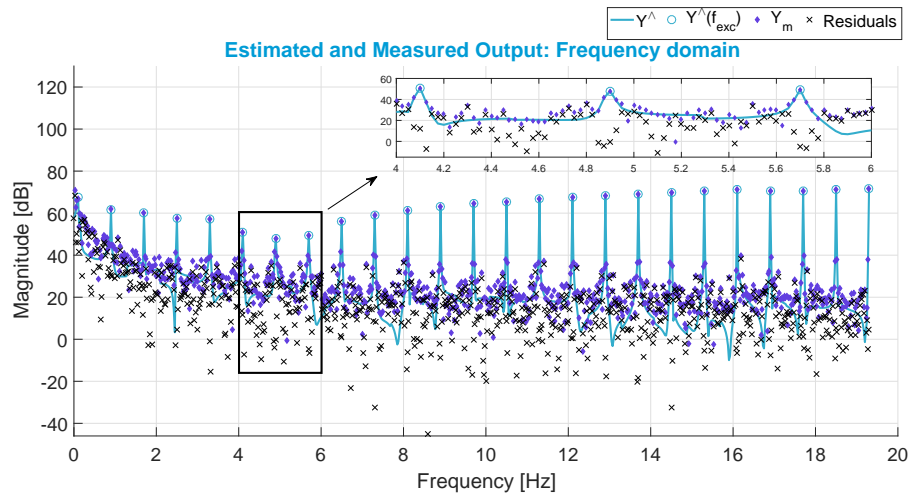


Figure 15: Fit in frequency domain from subject SIII, Slow Sine condition and segment c_2 . The blue diamonds represent the spectra of the pre-processed output Y , the light blue continuous line represents the estimated output spectra \hat{Y} , and the black crosses the residuals.

it starts at 0° and reaches 180° at the high frequencies, with a transitory phase between 3 Hz and 5 Hz. The black lines in the figure, representing the evolution of the magnitude/phase of the excitation frequencies in time, show a varying behavior until around 8 Hz. Afterward, the lines are more or less constant. In Figure 17, the resonance frequency extracted from the system function is plotted over time. The resonance frequency has the appearance of a sinusoid with a period of 40 s, ranging from 4.1 Hz to 5.7 Hz. The shape of the sinusoid is fragmented, with a resolution of 0.9 Hz.

C. Discussion on experimental study

1) Effects of design parameters on experimental accuracy
 a) Percentage of MVC

Initially, the desired torque trajectory was selected to vary between 10% and 50% of the MVC. The choice was made to ensure a visible change of the operational point and the creation of well recognizable Skirts in the output spectrum. However, as it was seen in Figure 12, the output spectrum contained noise at the non-excited frequencies. The noise was masking the formation of the Skirts, hindering the application of the *Skirt Decomposition* method. It was hypothesized that the noise was partially related to badly posed experimental conditions, requesting a maximum percentage of the MVC

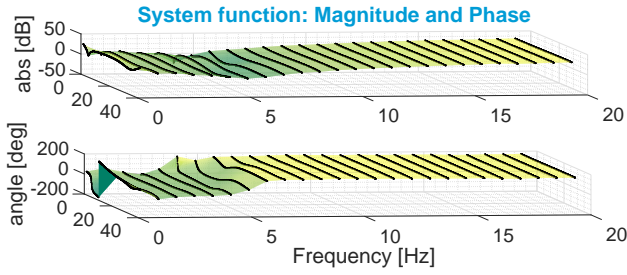


Figure 16: System function obtained from subject III, Slow Sine condition, segment c_2 . The top plot represents the absolute value in dB and the bottom plot the angle in degrees.

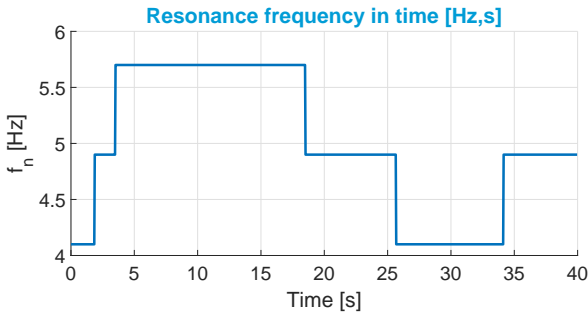


Figure 17: Resonance frequency in time for subject III, slow sine condition, segment c_2 . The property is retrieved from the system function.

that was too elevated. In fact, previous studies have reported a positive correlation between the force variability and the percentage of the MVC during isometric contractions in human joints [6], [7]. Therefore, for subject III the extreme percentages of the MVC were reduced to 5% and 20%.

The beneficial results brought by the decrease of the extreme values could already be noted in Figure 12, where the Skirts started to emerge around the excitation frequencies. Furthermore, positive effects on the estimation accuracy were observed in Table IV. The excursion between the minimum and maximum torque was reduced from 40% to 15%. Nevertheless, lowering the extreme percentages of the MVC was beneficial for the appearance of Skirts in the spectra and the application of the *Skirt Decomposition* method.

b) Subtraction of voluntary torque from the measured output

The output signal utilized in the data analysis was $y_\theta(t)$. The signal was obtained by subtracting an estimate of the voluntary torque from the measured output (Figure 10). The removal of the voluntary torque was crucial for the occurrence of the Skirts in the output spectrum. As it was seen in panel b of Figure 13, for the sawtooth condition the spectrum computed directly from the measured output presented a large Skirt centered at the origin. The large bandwidth Skirt covered the individual Skirts centered at the excitation frequencies, which

instead appeared when only $y_\theta(t)$ was used. The Skirt centered at the origin was interpreted as being caused by the contribution of the voluntary torque. Indeed, the shape corresponded to the Fourier transform of a ramp in the sawtooth trajectory.

The subtraction of the voluntary torque made sense under a physiological point of view. The two signals $y_v(t)$ and $y_\theta(t)$ are determined by two different physiological mechanisms [24] (Figure 10). The first mechanism is related to the tracking of the desired torque trajectory. The subjects received visual feedback on the desired output trajectory and the applied torque. To minimize the error between the signals, the subjects voluntarily changed the muscular activation level, with effects on joint admittance. During the tracking task, a position perturbation was applied to the joint. The related output $y_\theta(t)$ was determined by the value of joint admittance. Under this perspective, the output $y_\theta(t)$ can be considered as being LTV. The value of admittance was indeed modified in time by the voluntary tracking of the desired trajectory. The voluntary torque was required for the presence of time variation in the system, albeit it should not be considered for the identification.

c) Number of basis function

The method was applied by employing both a $zero^{th}$ order basis function and higher order basis functions. In the simulation study, it was explained that the width of the pre-determined Skirts is related to the number of basis functions adopted. When only one basis function is used, the relative Skirt in the frequency domain is reduced to a single peak at the origin. Therefore, the implementation of the *Skirt Decomposition* method with $N_p = 1$ corresponded to performing the identification at the excitation frequencies only.

In Table IV, it was seen that a high estimation accuracy was obtained using a $zero^{th}$ order analysis with data from the relax condition. The outcome was expected since for the relax condition the subjects were completing a LTI task. Performing the identification only at the excitation frequencies was sufficient to retrieve the dynamics of the system. For the other conditions, the 0^{th} order analysis resulted in a drop of accuracy, while the performance stayed high for $N_p > 1$. The result shows that it was advantageous for the identification to include the non-excited frequencies. The outcome supports the interpretation of joint admittance as being LTV and emphasizes the importance of considering the non-excited frequencies in the identification of LTV systems.

To best consider the non-excited frequencies, the number of basis functions should be selected taking into consideration the time variation. For subjects I and II, the desired torque trajectory ranged from 10% to 50% of the MVC, entailing an elevated rate of change for the time variation. Consequently, to enhance the approximation power, the value of N_p should be kept high. On the other hand, to avoid over-fitting of the noise and ensure the recognition of the Skirts, the maximum threshold was constrained to 8. For subject III, the amplitude of the desired torque trajectory was decreased, lowering the rate of change of the time variation. Therefore, the number of basis functions was reduced to 5.

2) Model interpretation

A common behavior in the frequency-magnitude plane of the system function could be extracted from Figure 16. The curve

that was obtained expressed how the system would behave if the properties were constant and 'frozen' at the relative time instance. Essentially, the curve represents a LTI response. For frequencies until around 16 Hz, the shape obtained corresponded to the response of a second-order LTI system, with resonance frequency around 5 Hz, and the phase was going from 0° to 180° . The plateau at the higher frequencies can be explained by the effects of the hand grip on the handle of the manipulator. As it was expected, the plot represents the inverse of the admittance, e.g. impedance. Indeed, conversely to the simulation study, the input and output were position and torque signals, respectively. The extracted dynamics are comparable to previous studies on LTI wrist impedance during force tasks [33]. In Figure 16 it was observed that the black lines, representing the evolution of the amplitude/phase of the frequencies in time, were varying until around 8 Hz. The outcome was predictable since for higher frequencies the constant inertia is dominant. The resonance frequency extracted from the system function was depicted in Figure 17. The resolution of the retrieved property was limited by the value of Δf_{exc} since the system function was obtained at the excitation frequencies only. However, it was possible to see a change of the resonance frequency in time. Particularly, the sinusoidal shape retrieved has an evident match with the shape of the imposed torque trajectory. The outcome confirms that the tracking task had a strong effect on the time variation.

3) Accuracy of the method

As it was seen in Figures 12, in the output spectra of the tracking tasks the power at the non-excited frequencies was at times as high as the power at the excitation frequencies. For example, for the intermediate sine condition, the power at the non-excited frequencies had an average value around 40 dB, almost 20 dB higher than for the relax condition. The power at the non-excited frequencies was interpreted as being partially due to noise and variability in the output. To reduce the level of the variability, the extremes values of the MVC were lowered. The change of the parameter was beneficial for the accuracy; in Table IV a net increase of the performance for subject III was observed.

The difference in the performance between the conditions tested on subject III can be partially explained by the diversity in complexity and speed of the time variation. When the speed/complexity of the time variation is low, the power of the Skirts is concentrated over a limited bandwidth. Therefore, the power of the Skirts at the individual frequencies becomes more dominant than the power of the noise. For the slow sine conditions, segments of 40 and 20 s were considered. The 40 s segments corresponded to a full period of the sinusoidal trajectory, and the 20 s segments to half a period. The complexity of the first case was higher, explaining the lower performance with respect to the 20 s segments.

In the time domain, a clear fit of the estimated output was observed in Figure 14. However, in the frequency domain, the fit was heterogeneous, displaying unevenly distributed residuals throughout the bandwidth (Figure 15). The distribution of the residuals can be partially explained by the shape of the output spectra. The considerable power at the non-excited frequencies in the bandwidth between 0 Hz and 2 Hz was

probably due to the discontinuities of the generated torque. Since the Skirts only model smooth contributions, the residuals at the low frequencies were large. From the output spectra, it was also pointed out that the noise was dominant at frequencies far from the excitation frequencies. Similarly, in these points, the residuals stayed high. Furthermore, the residuals might have been determined as well by unmodeled nonlinear dynamics. Finally, it was noticed that Skirts were visible around the excitation frequencies. In this limited bandwidth, the time variation was indeed dominant, and predetermined Skirts could be fitted to the output spectra. The relative residuals dropped consequently.

The drop in accuracy in the validation study was expected. Even for trials in which the desired trajectory was the same, it is likely that the tracking behavior of the subjects was not consistent over trials. As stressed in the introduction, humans are unpredictable, and their behavior has little repeatability. It follows that the operational point in time might be inconsistent over the trials. The LTV system function obtained for one trial might be different than for a different trial. The VAF was affected by the variability since the discontinuities of the voluntary torque were still present. Similarly, the residuals had a considerable increase with respect to the test set. However, when the residuals in the bandwidth 0.1-2 Hz were excluded from the calculation, it was noticed that the residuals dropped almost fivefold. From the validation results, it can be concluded that the model of joint admittance could describe the time-varying dynamics of the system for frequencies between 2 and 20 Hz.

D. Sub-conclusions on experimental study

Different conditions were tested to assess the performance of the *Skirt Decomposition* method on the identification of LTV joint admittance from human data. The comparison between the conditions provided important information regarding the design of a suitable experiment. It was seen that the variability within the system increased with the percentage of the MVC. When the desired torque trajectory was set to vary between 5% and 20%, it was possible to see a time variation in the system, while limiting the variability of the output. For future studies, it would be interesting to assess the performance of the *Skirt Decomposition* for different extremes of the MVC.

The role of the voluntary torque was discussed. The signal was required for the presence of the time variation within the system, yet it should be removed from the analyzed output. The signal might indeed overshadow the relevant Skirts around the excitation frequencies.

Finally, the accuracy of the method was analyzed. It was seen that the method could reconstruct the output in the time domain with a high accuracy. In the frequency domain, unevenly distributed residuals were observed. The estimation accuracy was high around the excitation frequencies, where the Skirts could form in the output spectra. Even though only a limited amount of point was used to reconstruct the smooth time variation of the system, this was sufficient to retrieve the time-varying dynamics of the system for frequencies higher than 2 Hz.

V. DISCUSSION

A. Time variation in the simulation and the experimental study

An essential difference between the simulation and the experimental study is that the simulation model was de facto LTV, while the joint dynamics were only modeled as being such. The time variation of the simulated model was indeed directly introduced by a change of the stiffness in time. Contrarily, in the experiment, the time variation was introduced by a change of the operational point. Time was used as a fictitious variable to explain the change of properties; considering the dynamics of the joint as being LTV was only a modeling trick.

In this study, the artifact used to introduce a time variation was to request to the subjects to track a desired torque trajectory. The relative voluntary torque was also part of the measured output. An estimate of the voluntary torque had to be obtained and subtracted from the measured output before applying the *Skirt Decomposition* method. Therefore, assumptions had to be made on the nature of the voluntary torque. The signal was considered as being linearly correlated to the desired torque trajectory. It was possible to estimate frequencies accurately above 2 Hz. Also, the task required to the subject was quite straightforward [31].

In literature, other factors of the operational point have been used to induce a time variation. In [17], the subjects were requested to maintain a constant torque level of their ankle, while a large amplitude angular perturbation was applied. The advantage was that the imposed joint angle could be measured exactly by the manipulator. However, the underlying task was quite challenging. In fact, it required a complex control of the activation level to guarantee a tracking of the desired torque trajectory for large variations of the angle. In [26], the subjects were requested to follow a predetermined trajectory for a desired angular position. In the studies, the manipulator applied a torque perturbation to the knee joint, while the output was the position of the joint in time. The task resulted as being more natural for the subjects [39]. However, the drawback was that the configuration between the manipulator and the humans was closed-loop. The identification method had to be modified accordingly.

To sum up, there exists no perfect experimental setup to study the time-variation of human joint dynamics. In this study, a force task was performed in which the subjects were asked to track the desired torque trajectory. Even though the voluntary torque was part of the measured output, it was possible to obtain an estimate of the signal and remove it from the analyzed data. Furthermore, the task resulted into an open-loop configuration between the joint and the manipulator and was intuitive for the subjects.

B. LTV identification of human joint admittance

The *Skirt Decomposition* belongs to the class of LTV identification methods. The aim of LTV methods is to build a model of the underlying system which takes into consideration the change of properties in time. For instance, in the *Skirt Decomposition* method, the non-parametric system function is built. The limitation of LTV methods is that, since the change of properties is expressed in function of time, it is not possible

to extrapolate the dynamics for a condition different than the one under test.

An alternative to LTV identification would be the use of Linear Parameter-Varying (LPV) methods. Conceptually, there is a strong similarity between LTV and LPV method: in both cases, time is the primary cause of the change of properties. However, in LPV methods, the dynamics are expressed in function of parameters that change in time, rather than time itself. The parameters introducing the time variation are known as scheduling functions. An important difference with the LTV cases is that the behavior of the underlying system can be extrapolated for novel trajectories of the scheduling functions. This property of LPV systems could be of great use for the application on the design of biomimetic prostheses.

For the simplified model tested in the simulation study, it would be possible to describe the system as being LPV. The time variation was introduced by the change of stiffness in time, and the stiffness could be selected as a scheduling function. On the other hand, the time variation of the human joint dynamics is more complex. With the current knowledge, it is still not possible to fully understand how the operational point affects human joint admittance [26]. Therefore, it is not possible to select the scheduling functions without risking modeling errors, and LPV methods cannot be applied.

In the presented study, a relation between the voluntary muscle torque and the joint dynamics was found. However, the results obtained were only for simple movements in which a small amplitude joint angle was imposed to the subjects. More research could be done for a wider set of movements to confirm the dependence of the dynamics on the voluntary torque. The *Skirt Decomposition* method could provide a tool for the research.

C. Skirt Decomposition method on human joint admittance

The *Skirt Decomposition* is a system identification method which applies nonparametric techniques for the identification of LTV systems. Due to the nonparametric structure, no *a priori* assumptions are made on the system's structure or order. Contrarily to the existing nonparametric LTV methods applied on human joint admittance, the *Skirt Decomposition* method does not require ensemble averaging over multiple realizations. Instead, it seizes the distinctive shape of the spectrum of linear slowly time-varying systems to fit predetermined Skirts. Essentially, the method reports the time variation properties onto the frequency domain, decreasing the number of unknowns in the system. Compared to the existing nonparametric methods, the *Skirt Decomposition* method does not require multiple trials with the same underlying time variation to build a LTV model. As it was seen from the experimental results, even for cases in which the tested condition was the same, the measured torque showed some variability. Assuming the repeatability of the time variation might result into less reliable identification outcomes. An added value to the use of a method that does not require ensemble averaging is that the experimental time is reduced.

Even though the *Skirt Decomposition* method has been previously applied to the identification of electric circuits,

its application on LTV human joint admittance was entirely novel. Transferring the method to this new application was not straightforward, particularly because joint admittance is less predictable, has more noise and has a lower bandwidth than electric circuits.

In the simulation study, it was seen that the difference in bandwidth was not a constraining factor. In fact, for each tested condition, it was possible to find the proper input and identification parameters to obtain a VAF greater than 90% and an RMSE of the resonance frequency lower than 0.1 Hz. The application of the method on human data proved challenging, especially due to the presence of noise at the non-excited frequencies. Nevertheless, close to the excitation peaks, it was possible to detect the Skirts. The fitting of a limited portion of the Skirts was sufficient to retrieve the time variation. The properties recovered from the system function showed plausible levels. The residuals had power between 16 and 27 for frequencies in the bandwidth between 2 and 20 Hz.

VI. CONCLUSIONS

A nonparametric approach for the identification of LTV joint admittance was proposed in this paper. Contrarily to the existing methods applied on LTV joint admittance identification, the *Skirt Decomposition* method did not require the control of the time variation and the parametrization of the LTV dynamics. From the simulation study, it was seen that the method was suitable for the identification of systems with dynamics similar joint admittance. In the human experiment, the method proved to be able to recognize the time variation, when an appropriate task was imposed and a proper bandwidth selected. The resonance frequency extracted from the system function showed a plausible time variation, following the shape of the desired torque trajectory.

REFERENCES

- [1] MIT, Mechanical Engineering Department. <http://ocw.mit.edu/courses/mechanical-engineering/2-017j-design-of-electromechanical-robotic-systems-fall-2009/course-text/MIT2017JF09ch02.pdf>. Accessed : 2016 - 03 - 01.
- [2] University of Tennessee, Medical department. <http://www.tiem.utk.edu/gross/bioed/webmodules/muscles.html>. Accessed: 2016-03-01.
- [3] Website of J. Lataire. <http://homepages.vub.ac.be/~jlataire/TVsystems/>. Accessed: 2016-01-04.
- [4] DJ Bennett, JM Hollerbach, Y Xu, and IW Hunter. Time-varying stiffness of human elbow joint during cyclic voluntary movement. *Experimental Brain Research*, 88(2):433–442, 1992.
- [5] B. Bigland-Richtie and J. Woods. Changes in muscle contractile properties and neural control during human muscular fatigue. *Muscle & nerve*, page 691, 1984.
- [6] LG Carlton and KM Newell. Force variability and characteristics of force production. *Variability and motor control*, pages 15–36, 1993.
- [7] Evangelos A Christou, Michael Grossman, and Les G Carlton. Modeling variability of force during isometric contractions of the quadriceps femoris. *Journal of motor behavior*, 34(1):67–81, 2002.
- [8] Erwin de Vlugt. An introduction to crossbow hunting. Lecture Slides for the course ‘System Identification and Parameter Estimation’, 2000.
- [9] Erwin De Vlugt, Alfred C Schouten, and Frans CT Van Der Helm. Adaptation of reflexive feedback during arm posture to different environments. *Biological cybernetics*, 87(1):10–26, 2002.
- [10] Kevin H Ha, Huseyin Atakan Varol, and Michael Goldfarb. Volitional control of a prosthetic knee using surface electromyography. *Biomedical Engineering, IEEE Transactions on*, 58(1):144–151, 2011.
- [11] John E Hall. *Guyton and Hall textbook of medical physiology*. Elsevier Health Sciences, 2015.
- [12] Neville Hogan. Adaptive control of mechanical impedance by coactivation of antagonist muscles. *Automatic Control, IEEE Transactions on*, 29(8):681–690, 1984.
- [13] HE Huxley. The mechanism of muscular contraction. *Science*, 164(3886):1356–1365, 1969.
- [14] MTV Johnson, AN Kipnis, MC Lee, and TJ Ebner. Independent control of reflex and volitional emg modulation during sinusoidal pursuit tracking in humans. *Experimental brain research*, 96(2):347–362, 1993.
- [15] Robert E Kearney, Richard B Stein, and Luckshman Parameswaran. Identification of intrinsic and reflex contributions to human ankle stiffness dynamics. *Biomedical Engineering, IEEE Transactions on*, 44(6):493–504, 1997.
- [16] RF Kirsch and RE Kearney. Identification of time-varying dynamics of the human triceps surae stretch reflex. ii. rapid imposed movement. *Experimental brain research*, 97(1):128, 1993.
- [17] Robert F Kirsch and Robert E Kearney. Identification of time-varying stiffness dynamics of the human ankle joint during an imposed movement. *Experimental brain research*, 114(1):71–85, 1997.
- [18] J Lataire. *Frequency domain measurement and identification of linear, time-varying systems*. PhD thesis, PhD thesis, Vrije Universiteit Brussel, University Press, Zelzate, 2011.
- [19] J Lataire, E Louarroudi, R Pintelon, and J Schoukens. Benchmark data on a linear time-and parameter-varying system.
- [20] John Lataire, Rik Pintelon, and Ebrahim Louarroudi. Non-parametric estimate of the system function of a time-varying system. *Automatica*, 48(4):666–672, 2012.
- [21] Hyunglae Lee and Neville Hogan. Time-varying ankle mechanical impedance during human locomotion. *IEEE Transactions on Neural Systems and Rehabilitation Engineering*, 23(5):755–764, 2015.
- [22] Ebrahim Louarroudi, John Lataire, Rik Pintelon, Pieter Janssens, and Jan Swevers. Frequency domain, parametric estimation of the evolution of the time-varying dynamics of periodically time-varying systems from noisy input–output observations. *Mechanical Systems and Signal Processing*, 47(1):151–174, 2014.
- [23] Ebrahim Louarroudi, Rik Pintelon, and John Lataire. Nonparametric tracking of the time-varying dynamics of weakly nonlinear periodically time-varying systems using periodic inputs. *Instrumentation and Measurement, IEEE Transactions on*, 61(5):1384–1394, 2012.
- [24] Daniel Ludvig and Robert E Kearney. Real-time estimation of intrinsic and reflex stiffness. *Biomedical Engineering, IEEE Transactions on*, 54(10):1875–1884, 2007.
- [25] Daniel Ludvig and Eric J Perreault. System identification of physiological systems using short data segments. *Biomedical Engineering, IEEE Transactions on*, 59(12):3541–3549, 2012.
- [26] Daniel Ludvig and Eric J Perreault. Task-relevant adaptation of musculoskeletal impedance during posture and movement. In *American Control Conference (ACC), 2014*, pages 4784–4789. IEEE, 2014.
- [27] Daniel Ludvig, Serge Pfeifer, Xiao Hu, and Eric J Perreault. Time-varying system identification for understanding the control of human knee impedance. In *System Identification*, volume 16, pages 1306–1310, 2012.
- [28] J Bart MacNeil, Robert E Kearney, and Ian W Hunter. Identification of time-varying biological systems from ensemble data (joint dynamics application). *Biomedical Engineering, IEEE Transactions on*, 39(12):1213–1225, 1992.
- [29] MM Mirbagheri, H Barbeau, and RE Kearney. Intrinsic and reflex contributions to human ankle stiffness: variation with activation level and position. *Experimental Brain Research*, 135(4):423–436, 2000.
- [30] Babak Moaveni and Eliyar Asgari. Deterministic-stochastic subspace identification method for identification of nonlinear structures as time-

- varying linear systems. *Mechanical Systems and Signal Processing*, 31:40–55, 2012.
- [31] Wilfred Mugge. *Reflex mechanisms in CRPS-related dystonia*. TU Delft, Delft University of Technology, 2011.
- [32] Winfred Mugge, Alexander G Munts, Alfred C Schouten, and Frans CT Van der Helm. Modeling movement disorderscrps-related dystonia explained by abnormal proprioceptive reflexes. *Journal of biomechanics*, 45(1):90–98, 2012.
- [33] Winfred Mugge, Alfred C Schouten, Jacobus J van Hilten, and Frans CT van der Helm. Impaired inhibitory force feedback in fixed dystonia. *IEEE Transactions on Neural Systems and Rehabilitation Engineering*, 24(4):475–484, 2016.
- [34] Winfred Mugge, Frans CT van der Helm, and Alfred C Schouten. Integration of sensory force feedback is disturbed in crps-related dystonia. *PLoS one*, 8(3):e60293, 2013.
- [35] Elliott J Rouse, Levi J Hargrove, Eric J Perreault, and Todd A Kuiken. Estimation of human ankle impedance during the stance phase of walking. *Neural Systems and Rehabilitation Engineering, IEEE Transactions on*, 22(4):870–878, 2014.
- [36] AC Schouten, WJT Van de Beek, JJ Van Hilten, and FCT Van der Helm. Proprioceptive reflexes in patients with reflex sympathetic dystrophy. *Experimental brain research*, 151(1):1–8, 2003.
- [37] Alfred C Schouten, Erwin de Vlugt, JJ Bob van Hilten, and Frans CT van der Helm. Design of a torque-controlled manipulator to analyse the admittance of the wrist joint. *Journal of neuroscience methods*, 154(1):134–141, 2006.
- [38] Alfred C Schouten, Winfred Mugge, and Frans CT van der Helm. Nmclab, a model to assess the contributions of muscle visco-elasticity and afferent feedback to joint dynamics. *Journal of biomechanics*, 41(8):1659–1667, 2008.
- [39] Alfred Christiaan Schouten. *Proprioceptive reflexes and neurological disorders*. TU Delft, Delft University of Technology, 2004.
- [40] Ehsan Sobhani Tehrani, Kian Jalaieiddini, and Robert E Kearney. Linear parameter varying identification of ankle joint intrinsic stiffness during imposed walking movements. In *Engineering in Medicine and Biology Society (EMBC), 2013 35th Annual International Conference of the IEEE*, pages 4923–4927. IEEE, 2013.
- [41] Richard B Stein and Robert E Kearney. Nonlinear behavior of muscle reflexes at the human ankle joint. *Journal of Neurophysiology*, 73(1):65–72, 1995.
- [42] Emanuel Todorov. Optimality principles in sensorimotor control. *Nature neuroscience*, 7(9):907–915, 2004.
- [43] Frans CT Van der Helm, Alfred C Schouten, Erwin de Vlugt, and Guido G Brouwn. Identification of intrinsic and reflexive components of human arm dynamics during postural control. *Journal of neuroscience methods*, 119(1):1–14, 2002.
- [44] Michel Verhaegen and Xiaode Yu. A class of subspace model identification algorithms to identify periodically and arbitrarily time-varying systems. *Automatica*, 31(2):201–216, 1995.
- [45] Martijn Vlaar, Teodoro Solis-Escalante, Alistair Vardy, Frans Van der Helm, and Alfred Schouten. Quantifying nonlinear contributions to cortical responses evoked by continuous wrist manipulation. *IEEE Transactions on Neural Systems and Rehabilitation Engineering*, 2016.
- [46] Martijn P Vlaar and Alfred C Schouten. System identification for human motion control. In *Instrumentation and Measurement Technology Conference (I2MTC), 2015 IEEE International*, pages 600–605. IEEE, 2015.
- [47] David T Westwick and Robert E Kearney. *Identification of nonlinear physiological systems*, volume 7. John Wiley & Sons, 2003.

- -0

Appendix A

Nonlinear Joint Admittance and Identification

A. Physiology of joint admittance

1) Intrinsic and reflexive properties

The admittance of a joint shows both *intrinsic* and *reflexive* properties. The intrinsic properties are related to the inherent physiological characteristics of the structures that compose and mobilize the joint and are mainly determined by inertial, viscous and elastic contributions. The inertial effect is linked to the geometrical configuration and to the mass distribution of the structures that are distal to the joint, while the viscous and elastic effects are associated with the mechanical characteristics of the muscles and of the passive tissues that cross the joint [43]. The intrinsic properties can be modulated to counteract the action of external disturbances with a mechanism known as *co-contraction*. It consists in the voluntary contraction of both the antagonist and the agonist muscles of a joint, resulting in an augmented visco-elasticity [43], hence in an increase in the admittance of the joint. The reflexive properties of joint admittance emerge from an unconscious mechanism to counteract disturbances. The initiators of the mechanism are the *proprioceptive sensors*, located in the muscles and the tendons. When disturbances are present, the sensors perceive a change of state (position, velocity, force) of the fibers to which they are attached, and they send a neural signal in response. The signal is transmitted to the brain and/or to the spinal cord, and again back to the muscles, where it can either activate or inhibit the target muscles. These two mechanisms can simultaneously affect admittance and therefore distinguishing their discrete effect might remain undetermined.

The contraction of sarcomeres is triggered by an action potential along the neural fibers, which is propagated in the muscular fibers, determining the release of calcium ions into the cells. The presence of the calcium ions induces a configurational change of the cross-bridges, allowing the relative sliding of the rows of actin and myosin, and resulting in a shortening of the sarcomeres, hence in a shortening of the overall muscle.

The force generated during contraction is dependent on the activation level, determined by the amount of calcium ions released into the muscular cell: the higher the activation level, the greater the probability that the cross-bridges undergo the configurational change necessary for contraction [31]. Given a constant activation level, the active force of a muscle also depends on the initial length of the muscle and the velocity of muscular contraction, as depicted in Figure 2. The force of the muscle changes with its initial length as the number of cross-bridges available for binding is different according to on the degree of overlap between the parallel fibers of actin and myosin. Furthermore, if the fibers completely overlap there is not sufficient room for the relative displacement of the fibers and the contraction cannot occur. The contractile force depends as well on the rate of change of muscular length. It is believed that the unbinding of cross bridges is facilitated when the muscle is shortening [13], [39]. For small deviations around a fixed operational point, the force-length-velocity relationship of Figure 2 can be linearized, and the force can be expressed as a linear function of a viscous and elastic constant [31]. Additionally, the force generated depends on the precedent muscular contractions. If in a short time lapse a muscle is contracted for the second time, the maximal force that it can generate is higher than the maximal force for the first contraction. The effect is known as *Treppe* effect, and it is caused by the fact that some calcium ions are still present in the cell from the previous action potential. On the other hand, for prolonged muscular contractions, muscular fatigue occurs, which reduces the maximal force that can be produced. Muscular fatigue is probably caused by the exhaustion of the available nutrients necessary for contraction [11].

2) Muscular contraction

The cells in a muscle are composed by multiple, consecutive sarcomeres which are the fundamental contractile units of a muscle. A sarcomere is composed of proteic filaments of actin and myosin, which form parallel, alternate rows connected by structures named cross-bridges, as shown in Figure 1.

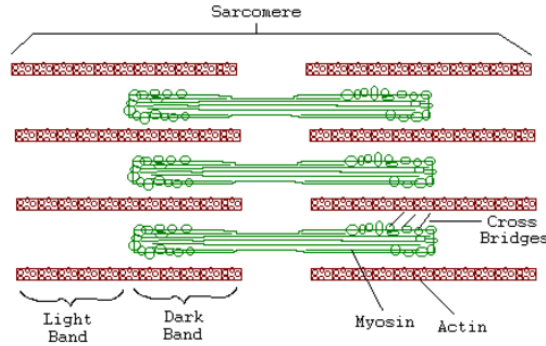


Figure 1: Schematic representation of the actin and myosin filaments in a sarcomere [2].

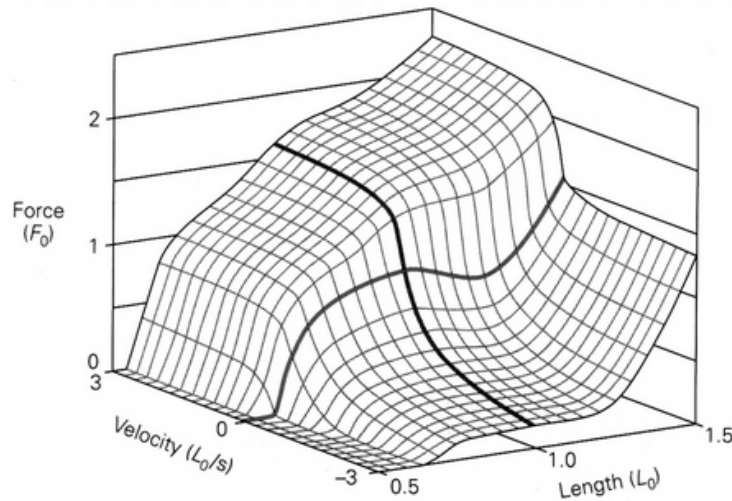


Figure 2: Graphical representation of the force-length-velocity relationship of a muscle [39].

B. Identification of joint admittance

1) Experimental setup

Joint admittance can be estimated by applying system identification procedures on joint measurements. The measurements can be obtained experimentally by the utilization of robotic devices, named manipulators. The manipulators should perturb the joint of the human subjects and be equipped with sensors for the measurement of the joint response. The signal that the manipulator imposes to the joint is known as *perturbation signal*. The interaction between the human subjects and the manipulators for the estimation of the joint admittance is schematized in Figure ???. The manipulator traces a pre-defined angle and generates an angular perturbation, which is measured by sensors and used as input for the identification procedure.

The manipulator acts as a position servo which controls the angular position of the joint. The resulting torque generated by the joint is measured and used as output for the identification. The measurements of the input and output signals are noisy and do not exactly correspond to the actual ones; the error is modeled as random, additive noise, named *input/output measurement noise* respectively. The input and output measurement noises are assumed to be statistically independent of the output of the system [47]. The variability within the system is modeled as additive, *process noise*. The manipulator has a stiffness which is much higher than the stiffness of the joint of the human subject. Consequently, the torque produced at the joint does not affect the position of the manipulator, and it is only measured by the device. Accordingly, the interaction between the human and the manipulator is an open-loop one. Oppositely, if the manipulator is designed as being compliant, the torque generated by the subject had an effect on the manipulator, and the relationship is no longer in open-loop.

There are three main types of tasks that the subjects can perform in an experiment for joint admittance identification: position tasks, force tasks, and relax tasks [31]. In position tasks, the subjects are asked to keep the joint at a fixed angle, while the joint is perturbed by the manipulator. To minimize position deviation, the subjects increase their admittance level. In force tasks, the subjects are asked to exert a constant force regardless of the position. In this case, the joint is kept compliant to minimize the force deviations. Finally, in relax tasks the subjects are asked to remain passive, and the only component of admittance that can be identified are the passive properties of the muscles and the other tissues.

2) Challenges

There are some challenges that are present when identification procedures are performed on human subjects:

- The control behavior of a human is susceptible to several changes, dictated for instance by a different planning, a change in external conditions or task demands. Humans adjust their control behavior and the central nervous system can learn the optimal control setting to apply to a certain motor task.
- The muscular system of humans is redundant, and it is possible to perform the same movement by engaging different muscles. For the same experimental conditions, different muscles can, therefore, be employed.
- For experiments that are physically challenging or that require a long recording time, it is likely that the behavior of the subject changes due to fatigue and boredom. If muscular fatigue occurs, the maximal speed of muscular contraction and the maximal contraction level decrease [5]. To avoid fatigue, the experimental time should be constrained.
- Human neuromuscular system is composed of several elements that cooperate for an optimal functioning. When a component of the system is studied, it is possible that more or less predictable effect by adjacent structures can affect the behavior of the component. The lack of modularity renders the study of the neuromuscular system more complex since it is not straightforward to split up the problem in smaller ones.
- The force generated by a muscle is nonlinear, and it is affected by multiple factors, which have to be considered during the identification procedures.

Appendix B

LTV systems

A. Definition

By definition, a system is time-varying when a time-shifted version of the response does not correspond to the response to the input shifted by the same amount [1]. In mathematical form, a time-varying system is such that [47], given:

$$y(t) = f(u(t))$$

then:

$$y(t - \tau) \neq f(u(t - \tau)) \tag{8}$$

where:

- t is the time vector;
- τ is the time-shift factor;
- $y(\cdot)$ is the output (response) of the system and $u(\cdot)$ is the input of the system;
- $f(\cdot)$ is a generic function expressing the dynamics of the system.

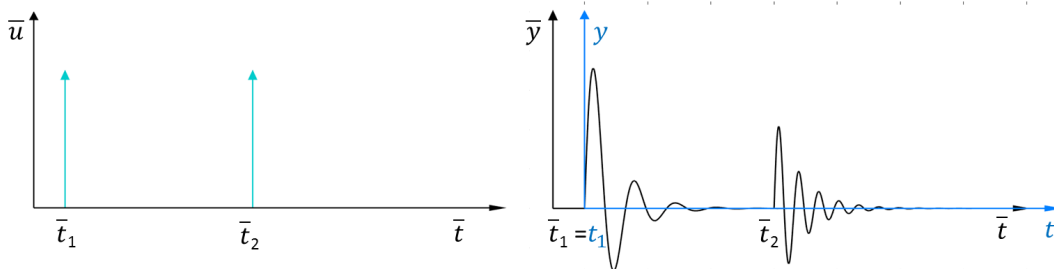


Figure 1: Example of the response (right) of a time-varying system to two consecutive impulses of equal magnitude (left) [18].

In other words, a system is time-varying if its response depends on the time instance in which the input is applied. An example is given by Figure 1, which represents the response of a system to two consequent impulses of equal magnitude. The first impulse is applied at $\bar{t} = \bar{t}_1$, and the response resembles that of a second-order system with fixed parameters. The second impulse is applied at $\bar{t} = \bar{t}_2$, when the response to the first input has virtually completely vanished [18]. Again, the response resembles that of a time-invariant second-order system, although it is different from the response to the impulse applied at \bar{t}_1 .

1) Cause of the time variation

There are two distinct ways in which time variation can occur in a system. There are systems which are intrinsically time-varying and for which the cause of the change of the properties in time lies in the random nature of the system. Examples are chemical processes or pitting corrosion in metals [22]. In other systems, the time variation is externally induced and is caused by the change in time of one or more external factors that influence the system [22]. An example is an electric circuit in which the battery of the external power supply is progressively decaying, affecting the properties of the circuit. For both the intrinsic and the externally induced case, the passing of time is the driving variable that causes, directly or indirectly, the change of properties. Moreover, it is possible to treat a nonlinear time-invariant system as a linear time-varying system so that linear methods can be applied for identification. The translation from

nonlinear time-invariant system to linear time-varying system can be done by linearizing the system around time itself. Time is not the driving variable for the change of properties, although it can be considered as a fictitious variable of the system and the nonlinear time-invariant systems can be treated as a LTV in which the time variation is externally induced.

B. Response

1) Impulse response function

When building the impulse response function of a LTV system, the dependence to time is taken into consideration, resulting in a function of two variable: $g_v(t, \bar{t})$. The variable \bar{t} represents the time instance in which the impulse is applied, while the variable t represents the time elapsed from the beginning of the measurements. The variable \bar{t} is defined in an absolute reference frame; for instance, it could be the clock time or the time of a stopwatch started at the beginning of the measurements. The variable t is defined on a relative time frame, in which the zero is correspondent to the time in which the signal has started being measured. The variable \bar{t} is named absolute time, and it is defined by the black axes in Figure 1, the variable t is named observational time, and it is defined by the blue axes in Figure 1. For computational simplicity, it is common practice to have the origin of the axes for the absolute time coincide with the origin of the axes for relative time, which results into $\bar{t} = t$ and $g_v(t, t)$.

The time-varying (causal) impulse response represents the dynamics of the system and can be used to reconstruct its output using convolution with the system input as following:

$$y(t) = \int_0^t g_v(\tau, t) u(t - \tau) d\tau \quad (9)$$

where:

- $y(t)$ and $u(t)$ are the respectively the output and input signals.
- The begin of measurement is considered as zero for the absolute frame and \bar{t} is taken as $= t$.
- $g_v(\tau, t)$ is the time-varying impulse response at observation time τ and absolute time t .

An important consequence of the variation in time of the impulse response is the fact that the characteristics of the system, such as the rise time and the settling time, depend on the dynamics of the system and also by the time instance in which the input is applied.

2) Sinusoidal response

By applying a co-sinusoidal input $u(t) = \cos(\omega t)$ with angular frequency ω to a LTV system, described as in Equation 9, the output becomes:

$$y(t) = \int_0^\infty g_v(\tau, t) \cos(\omega(t - \tau)) d\tau - \int_t^\infty g_v(\tau, t) \cos(\omega(t - \tau)) d\tau \quad (10)$$

where:

- The first integral represents $y_{ss}(t)$, the steady-state response to the co-sinusoid signal;
- The second integral represents $y_{tr}(t)$, the transient response.

It is possible to rewrite Equation 10 using Euler formula for cosine signals. If, for the sake of simplicity, the formula is only applied to $y_{ss}(t)$, the resulting expression is:

$$\begin{aligned}
 y_{ss}(t) &= \frac{1}{2} \int_0^\infty g_v(\tau, t) e^{j\omega(t-\tau)} d\tau + \frac{1}{2} \int_0^\infty g_v(\tau, t) e^{-j\omega(t-\tau)} d\tau = \\
 &= \frac{1}{2} e^{j\omega t} \int_0^\infty g_v(\tau, t) e^{-j\omega\tau} d\tau + \frac{1}{2} e^{-j\omega t} \int_0^\infty g_v(\tau, t) e^{j\omega\tau} d\tau = \\
 &= \frac{1}{2} e^{j\omega t} G_v(j\omega, t) + \frac{1}{2} e^{-j\omega t} G_v(-j\omega, t) = \\
 &= \Re(G_v(j\omega, t)) \cos(\omega t) - \Im(G_v(j\omega, t)) \sin(\omega t) = \\
 &= |G_v(j\omega, t)| \cos(j\omega t + \angle G_v(j\omega, t))
 \end{aligned} \tag{11}$$

where:

- $G(j\omega, t)$ is the Fourier transform of the time-varying impulse response $g_v(\tau, t)$, $|G(j\omega, t)|$ is its absolute value and $\angle G(j\omega, t)$ its phase ;
- The input is rewritten using the Euler formula $u(t) = \frac{e^{j\omega t} + e^{-j\omega t}}{2}$.

Contrarily to LTI systems, applying a sinusoidal input with a fixed frequency to a LTV system does not result in a pure sinusoidal steady-state response. As it can be seen in Equation 11, the response is instead a multiplication of a function dependent on time $|G_v(j\omega, t)|$ with a co-sinusoidal function with variable phase $\cos(j\omega t + \angle G_v(j\omega, t))$. For a constant $G_v(j\omega, t)$, the output is a co-sinusoidal signal with fixed amplitude and phase, getting back to a LTI system. If there is no noise in the system, the LTI output spectrum has power only at the frequency excited by the input, and its magnitude only has a peak at the excitation frequency. For a slowly varying $G_v(j\omega, t)$, the output is a cosine signal with an amplitude and a phase that slowly change over time. The resulting output spectra still has most of the power at the input frequency; yet, the neighboring frequencies are also excited. The resulting spectrum has a 'Skirt-like' shape, and this property will be used for identification using the 'Skirt decomposition method'.

3) Response to a multisine signal

The expression $G_v(j\omega, t)$ is linear in its argument, and if the sum of N co-sinusoidal signals with angular frequency ω_k and amplitude a_k is applied to the system, then the resulting output is:

$$y_{ss}(t) = \sum_{k=1}^N (|G_v(j\omega_k, t)| \cos(j\omega_k t + \angle G_v(j\omega_k, t))) \tag{12}$$

C. Nonparametric model

1) LTV system function

As seen in Equation 11, by taking the Fourier transform of the time-varying impulse response in Equation 9, the time-varying system function $G_v(s, t)$ is obtained as following:

$$G_v(j\omega, t) = \int_0^\infty g_v(\tau, t) e^{-j\omega\tau} d\tau \tag{13}$$

The system function represents the dynamics of a LTV system under both a time-domain and frequency-domain profile. In Figure 2 the magnitude of a time-varying system function is represented. By looking at the figure at a fixed time instance, a typical frequency response of a LTI second-order system can be recognized. By looking at the picture in the time-magnitude plane, the evolution of the properties of the system in time is represented. For example, it is possible to see how the resonance frequency changes throughout the response. The output in time-domain can be rewritten by taking the inverse Fourier transform of the system function multiplied by the inverse spectra, as following:

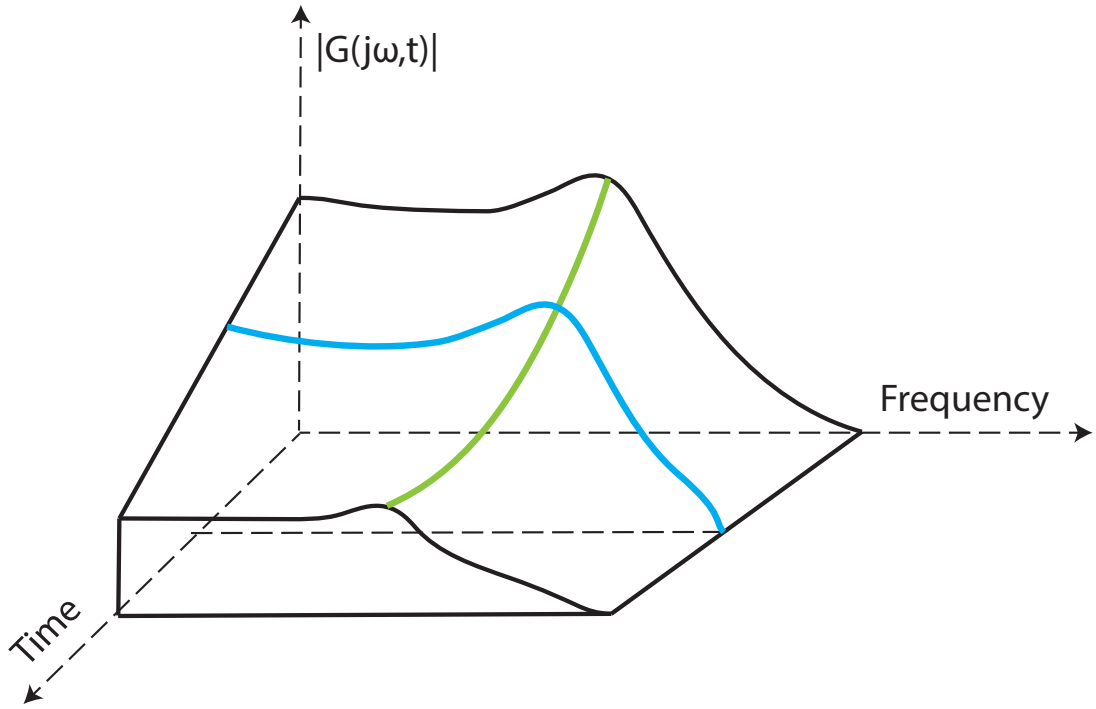


Figure 2: Graphical example of the magnitude of a LTV system. The green line shows the evolution of the resonance frequency in time, the blue line shows the frequency response at a fixed time instant.

$$y_{ss}(t) = \mathcal{F}^{-1}(G_v(j\omega, t)U(j\omega)) \quad (14)$$

2) Polynomial decomposition

The system function $G_v(j\omega, t)$ can be decomposed as a series expansion, in which the time-domain and frequency-domain profiles are represented by distinguished functions:

$$G_v(j\omega, t) = \sum_{p=0}^{N_p-1} G_p(j\omega)b_p(t) \quad (15)$$

where:

- The frequency dynamics are represented by the LTI functions $G_p(j\omega)$, and the time variation is represented by the polynomials $b_p(t)$, known as *basis functions*;
- N_p represents the number of basis functions used, while $N_p - 1$ represents the order of the series expansion;
- It is assumed that the system function can be approximated by a finite number of smooth basis functions of time $b_p(t)$;

By combining Equations 14 and 15 the output of a time-varying system becomes:

$$\begin{aligned} y_{ss}(t) &= \sum_{p=0}^{N_p-1} \mathcal{F}^{-1}(G_p(j\omega)U(j\omega))b_p(t) \\ &= \sum_{p=0}^{N_p-1} \mathcal{F}^{-1}(\theta_p(j\omega))b_p(t) \end{aligned} \quad (16)$$

where:

- \mathcal{F}^{-1} is the inverse Fourier operator;
- $\theta_p(j\omega)$ is a LTI variable introduced to substitute $\frac{1}{2\pi}G_p(j\omega)U(j\omega)$.

The expression can be interpreted as a LTI Multiple-Input Single-Output (MISO) system. Each of the N_p inputs is determined by the Fourier transform of $(\theta_p(j\omega))$, each subsystem is represented by a multiplication of the input with the polynomial $b_p(t)$ retrieving the steady-state LTV output $y_p(t)$. Finally, the steady-state LTV outputs of each subsystem are summed together to obtain $y_{ss}(t)$.

The expression in time domain in Equation 16 can be written in frequency domain:

$$Y_{ss}(j\omega) = \frac{1}{2\pi} \sum_{p=0}^{N_p-1} \theta_p(j\omega) * B_p(j\omega) \quad (17)$$

where:

- $B_p(j\omega)$ is the Fourier transform of $b_p(t)$;
- The multiplication operator in Equation 16 has become a convolution.

In Equation 17 the decomposition of the system as an LTI MISO output can still be recognized.

Appendix C

Skirt Decomposition Method

A. Multisine Input signal

The input utilized for the *Skirt Decomposition* method is a multisine signal, a continuous signal composed by the sum of N_{exc} co-sinusoids. The signal is defined as:

$$u_{ms}(t) = \sum_{k_e \in \mathbb{K}_{exc}} A(k_e) \cos(\omega_{k_e} t + \Phi_{k_e}) \quad (18)$$

The multisine signal is composed by the sum of N_{exc} co-sinusoids, each one with a given amplitude $A(k_e)$, a random phase Φ_{k_e} , and exciting an angular frequency ω_{k_e} . The multisine is defined over a period T_m . The excitation frequencies are designed such that the period of each individual co-sinusoid is a integer divisor of T_m . The set of excited angular frequencies is:

$$\omega_{k_e} = \frac{2\pi k_e}{T_m}, \text{ for } k_e \text{ integer and } \in \mathbb{K}_{exc}$$

The multisine signal allows for a higher power at the excitation frequencies compared to a signal with a flat spectrum. The SNR at the excitation frequencies is improved [45]. Furthermore, the multisine signals have the advantages of being a continuous, yet unpredictable signal. The multisine is particularly suitable for human experiments due to these properties [39]. Finally, the application of the multisine as input gives the possibility of selecting the frequencies to excite. The property is important for the *Skirt Decomposition* method since it requires a significant number of unexcited frequencies between two excited ones [20]. The Fourier transform of the multisine signal is expressed as $U_{ms}(j\omega_{k_e})$.

1) Properties of the multisine

The input signal is windowed, meaning that it is multiplied in the time domain by a rectangular window of length T , rendering the signal equal to zero for time points outside the window. The signal is sampled with a sample frequency f_s and it is band-limited. The set of discrete frequencies over which the signal is defined are:

$$\omega_k = \frac{2\pi k}{T}, \text{ for } k \in \mathbb{K}_w = [0 : \frac{T f_s}{2}) \cap \mathbb{Z} \quad (19)$$

For a sample frequency f_s , defining the multisine signal as above is required to avoid aliasing and leakage. Furthermore, as required by the *Skirt Decomposition* method, not all the frequencies in \mathbb{K}_w are excited by the multisine signal.

B. Rewriting the formula

For the application of the *Skirt Decomposition* method, the convolution in Equation 17 has to be rewritten in the form of matrix multiplication. First of all, the signal is discretized over the frequencies $\omega_k \in \mathbb{K}_w$ and the transient part of the response is added, obtaining:

$$Y(j\omega_k) = \sum_{p=0}^{N_p-1} \theta_{p,k'} * B_p(j\omega_k) + I_{tr}(j\omega_k) \quad (20)$$

where:

- The transient response is modeled by the polynomial $I_{tr}(j\omega_k)$,

- θ_p, k' represents the LTI component $1/(2\pi)G_p(j\omega_k)U_{ms}(j\omega_{k_e})$. Since the multisine U_{ms} is null at the non-excited frequencies, the multiplication with $G_p(j\omega_k)$ results into an expression which is defined only over the excitation frequencies.

Lets only considered $Y_p(j\omega_k)$, the output from a single branch of the equation. Transforming the convolution into multiplication, the following expression is obtained:

$$Y_p(j\omega_k) = \sum_{k' \in \mathbb{K}_{exc}} \theta_{p,k'} B_p(j\omega_{k-k'}) \quad (21)$$

where:

- $B_p(j\omega_{k-k'})$ is a Skirt centered at the frequency ω_{k_e} .

For the application of the *Skirt Decomposition* method, the equation has to be rewritten in matrix form. To minimize the computational effort, Equation 21 is split up into K_{exc} frequency bands composed by $N_c - 1$ elements. Each frequency band is centered around an excitation frequency ω_{k_e} and considers only the excitation frequency before $\omega_{k_e}^-$ and the excitation frequency after $\omega_{k_e}^+$. The frequency band is defined over the following points:

$$\omega_k \in F_{k_e} = \left[\omega_{k_e}^- - \frac{\omega_{k_e} - \omega_{k_e}^-}{2}, \omega_{k_e}^+ + \frac{\omega_{k_e} - \omega_{k_e}^+}{2} \right] \quad (22)$$

For each frequency band, only the Skirts centered at $\omega_{k_e}^-$, ω_{k_e} and $\omega_{k_e}^+$ are considered. The contribution of the neglected Skirts is modeled as a smooth polynomial, in function of $j\omega_k$. The expression obtained is:

$$Y_p(j\omega_k, k_e) = \sum_{k'=k_e^-, k_e, k_e^+} \theta_{p,k'} B_p(j\omega_{k-k'}) + I_{sm}(j\omega_k) \quad (23)$$

where:

- $Y_p(j\omega_k, \omega_{k_e})$ expresses the output, for a fixed branch p , computed over the frequencies $\omega_k \in F_{k_e}$, with central frequency ω_{k_e} .

Finally, summing over the N_p branches, the following expression is obtained:

$$Y(j\omega_k, k_e) = \sum_{k'=k_e^-, k_e, k_e^+} \sum_{p=0}^{N_p-1} \theta_{p,k'} B_p(j\omega_{k-k'}) + I_{tot}(j\omega_k) \quad (24)$$

where:

- $I_{tot}(j\omega_k)$ is a polynomial of order $N_{tr} + 1$ and in function of $j\omega_k$. The polynomials models both the transient part $I_{tr}(j\omega_k)$ and the smooth contribution from the neglected Skirts $I_{sm}(j\omega_k)$. The polynomial is represented as : $I_{tot}(j\omega_k) = \sum_{l=0}^{N_{tr}} tr_l(j\omega_k)^l$

For each frequency band, composed by $N_c - 1$ elements, of order $N_p - 1$ and an order of the transient $N_{tr} + 1$ the equation can now be written in matrix form, as:

$$Y(j\omega_k) = B(j\omega_k)\Theta(j\omega_{k_e}) \quad (25)$$

$$\begin{aligned}
 B(j\omega_k) &= \begin{pmatrix} B_0(j\omega_{k1-ke^-}) & B_0(j\omega_{k1-ke}) & B_0(j\omega_{k1-ke^+}) & \cdots & B_{Np-1}(j\omega_{k1-ke^+}) & j\omega_{k1}^0 & \cdots & j\omega_{k1}^{Ntr} \\ B_0(j\omega_{k2-ke^-}) & B_0(j\omega_{k2-ke}) & B_0(j\omega_{k2-ke^+}) & \cdots & B_{Np-1}(j\omega_{k2-ke^+}) & j\omega_{k2}^0 & \cdots & j\omega_{k2}^{Ntr} \\ \vdots & \vdots \\ B_0(j\omega_{Nc-ke^-}) & B_0(j\omega_{Nc-ke}) & B_0(j\omega_{Nc-ke^+}) & \cdots & B_{Np-1}(j\omega_{Nc-ke^+}) & j\omega_{kNtr}^0 & \cdots & j\omega_{kNtr}^{Ntr} \end{pmatrix} \\
 \Theta(j\omega_{ke}) &= \left(\theta_{0,ke^-} \quad \theta_{0,ke} \quad \theta_{0,ke^+} \quad \cdots \quad \theta_{Np-1,ke^+} \quad tr_0 \quad \cdots \quad tr_{Ntr} \right)^T
 \end{aligned} \tag{26}$$

C. Linear least-squares regression

For every frequency band, centered at the excitation frequency ω_{ke} a linear least-squares regression is applied to retrieve the vector $\Theta(j\omega_k)$ from Equation 25. The equation solved is:

$$\hat{\Theta}(j\omega_{ke}) = \min_{\Theta} \|Y_m(j\omega_k) - B(j\omega_k)\Theta(j\omega_{ke})\|_2^2 \tag{27}$$

where:

- The value $Y_m(j\omega_k)$ represents the measured output in the frequency domain.
- The frequencies considered are $\omega_k \in F_{ke}$.

By solving the linear least-squares regression for each frequency band, a set of N_{exc} vectors $\hat{\Theta}(j\omega_{ke})$ is obtained. From each vector $\hat{\Theta}(j\omega_{ke})$, only the terms relative to the central frequency ω_{ke} are retained. The LTI response at the excitation frequencies is obtained. The vector is equal to:

$$\theta_{ke} = [\theta_{0,ke1}, \theta_{1,ke1}, \dots, \theta_{Np-1,ke1}, \theta_{0,ke2}, \theta_{1,ke2}, \dots, \theta_{Np-1,ke2}, \dots, \theta_{Np-1,keN_{exc}}] \tag{28}$$

The vector contains $N_p \cdot N_{exc}$ elements. For a fixed branch, the vector is expressed as $\theta_{p,k'e}$.

D. Reconstruction of the LTV system function

The system function can be reconstructed from the LTI response, the input signal and the basis functions. As stated in Equation 15, the system function is the series expansion of the LTI functions $G_p(j\omega_k)$ and the basis functions. $G_p(j\omega_k)$ can be obtained by dividing the LTI response by the multisine input, giving the following expression for the system function:

$$G_v(j\omega_{ke}, t) = \sum_{p=0}^{Np-1} \frac{\theta_{p,k'e}}{U_{ms}(j\omega_{ke})} b_p(t) \tag{29}$$

E. Reconstruction of the output

The output can be estimated starting by multiplying the LTI response $\theta_{p,k'e}$, expressed in the time domain, by the basis functions. To express the LTI in the time domain, the vector is made of the desired dimension $N/2$, corresponding to the number of points up to the Nyquist frequency. To change the dimension, zeros are added at the non-excited frequencies. The vector is expressed in the time domain by performing an inverse Fourier transform, obtaining a time vector $\hat{\theta}_p(t)$. The output equals $\hat{y}(t) = \sum_{p=0}^{Np-1} \hat{\theta}_p(t) \cdot b_p(t)$.

When a validation set is used, a similar procedure can be followed to retrieve the estimate of the output.

The LTI response is retrieved in the frequency domain as:

$$G_p(j\omega_{ke}) = \sum_{p=0}^{N_p-1} \frac{\theta_{p,k'e}}{U_{ms}(j\omega_{ke})} U_{ms2}(j\omega_{ke}) \quad (30)$$

where $U_{ms2}(j\omega_{ke})$ is the input applied in the validation dataset. The estimated output is computed with the same procedure as above.

E. Assumptions

The main assumptions made by the *Skirt Decomposition* method are:

- 1) The basis functions $b_p(t)$ are smooth functions of time, and their Fourier transform have the power highly concentrated at low frequencies (Skirt shape).
- 2) The transient part of the response and the contribution of the Skirts that are not in the considered frequency band can be approximated by a polynomial in $j\omega_k$ of order N_{tr} .
- 3) The matrix $B(k)$ is non-singular.
- 4) The LTI systems G_1, \dots, G_{N_p} are asymptotically stable;
- 5) The input signal is bandlimited, and the excited frequencies are integer multiples of $2\pi/T_{exp}$, with a maximum excitation frequency of $f_s/2$, where T_{exp} is the experimental time, and f_s the sampling frequency.
- 6) The output is corrupted by random, circular complex, normal distributed, white noise.
- 7) There is no input noise.

Appendix D

Additional Figures and Tables

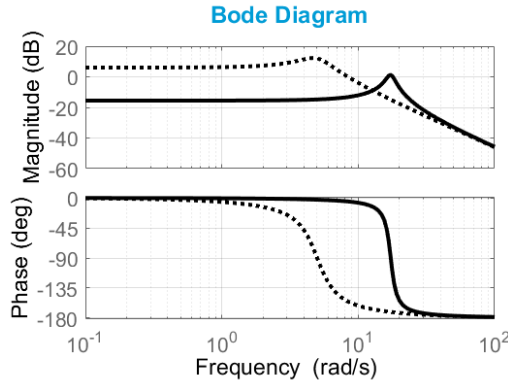


Figure 1: Bode plot of the implemented mass-spring-damper model in the simulation for $K = K_{max} = 6 \text{ Nm/rad}$ (black line) and $K = K_{min} = 0.5 \frac{\text{Nm}}{\text{rad}}$ (blue line). The inertia I_c is equal to $0.02 \frac{\text{Nm s}^2}{\text{rad}}$ and the damping B_c is equal to $0.05 \frac{\text{Nm s}}{\text{rad}}$

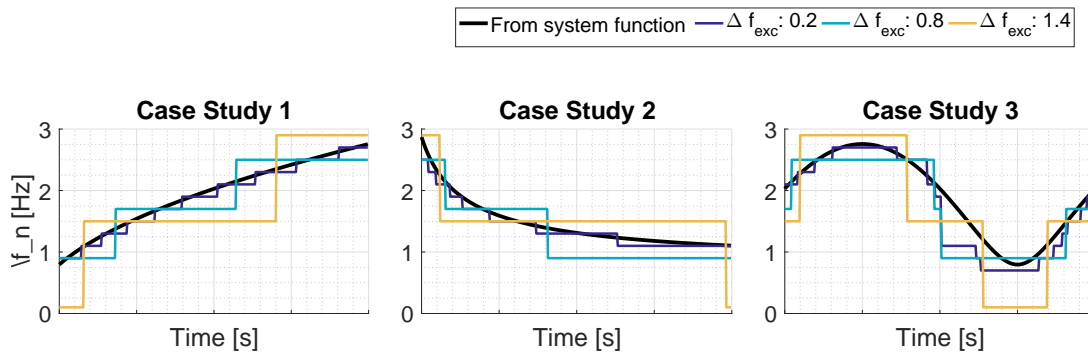


Figure 2: Resonance frequency from the Simulation on Case Studies 1, 2 and 3. The black line represents the resonance frequency of the system, while the colored lines represent the resonance frequency retrieved for different values of Δf_{exc}

